energies

MDPI

Article

Bioenergy from Maize Silage by Anaerobic Digestion: Batch Kinetics in Relation to Biochemical Composition

Krzysztof Pilarski [1,*], Agnieszka A. Pilarska [2,*], Michał B. Pietrzak [3] and Bartłomiej Igliński [4]

[1] Department of Biosystems Engineering, Poznań University of Life Sciences, Wojska Polskiego 50, 60-627 Poznań, Poland
[2] Department of Hydraulic and Sanitary Engineering, Poznań University of Life Sciences, ul. Piątkowska 94A, 60-649 Poznań, Poland
[3] Department of Statistics and Econometrics, Gdańsk University of Technology, ul. Gabriela Narutowicza 11/12, 80-233 Gdańsk, Poland; michal.pietrzak@pg.edu.pl
[4] Faculty of Chemistry, Nicolaus Copernicus University in Toruń, Gagarina 7, 87-100 Toruń, Poland; iglinski@chem.umk.pl
* Correspondence: krzysztof.pilarski@up.poznan.pl (K.P.); agnieszka.pilarska@up.poznan.pl (A.A.P.); Tel.: +48-61-846-65-93 (A.A.P.)

Abstract

Maize silage can play a key role in policies aimed at stabilising local energy systems, as it constitutes a critical renewable feedstock for European biogas plants. By providing a dense and predictable source of chemical energy, it supports balance and reliability in the agricultural energy sector. To convert this potential into stable energy production, operators require kinetic models that translate routine silage quality indicators into concrete guidance for digester operation and control. Therefore, the aim of this article was to evaluate the batch kinetics of anaerobic digestion (AD) of maize silage and to select an adequate model for describing biochemical methane potential (BMP) profiles and associated energy recovery in the context of start-up, organic loading rate (OLR), hydraulic retention time (HRT) and feedstock preparation. Ten batches of silage (A–J) were examined, covering a realistic range of pH, electrical conductivity (EC), dry and volatile solids, ash, protein–fat–fibre fractions, fibre composition (NDF, ADF and ADL), derived fractions (hemicellulose, cellulose, and residual organic matter (OM)), C/N ratio and macro-/micronutrient profiles, including trace elements relevant to methanogenesis (Ni, Co, Mo, and Se). BMP tests were carried out in batch mode, and the resulting curves were fitted using the modified Gompertz and a first-order kinetic model. Methane yields of approx. 100–120 m^3 CH_4/Mg fresh matter (FM) and 336–402 m^3 CH_4/Mg volatile solids (VS), with CH_4 contents of 52–57% v/v, were typical for energy-grade maize silage. Kinetic and energetic behaviours were governed mainly by residual OM and hemicellulose (shortening the lag phase and increasing the maximum methane production rate), the ADL/cellulose ratio (controlling the slower hydrolytic tail), EC and Na/Cl/S (extending the lag phase), and C/N together with Ni/Co/Mo/Se (stabilising methanogenesis). The modified Gompertz model reproduced BMP curves with a pronounced lag phase and asymmetry more accurately (lower error and better information criterion values), and its parameters directly support start-up design, OLR ramp-up and energetic performance optimisation in bioenergy reactors. The novelty of this work lies in combining batch BMP tests, comparative kinetic modelling and detailed silage characterisation to establish quantitative links between kinetic parameters and routine maize silage quality indicators that are directly relevant for biogas plant operation and renewable energy production.

Academic Editor: Alberto Maria Gambelli

Received: 12 January 2026
Revised: 17 February 2026
Accepted: 20 February 2026
Published: 22 February 2026

Keywords: agricultural energy sector; energy systems; bioenergy; maize silage; anaerobic digestion; biochemical methane potential (BMP); kinetic modelling; modified Gompertz model

1. Introduction

In recent years, maize silage has remained the most widely used feedstock in European anaerobic digestion (AD) plants and is widely applied in mixed feeding regimes due to its high energy density, predictable logistics, and comparatively low toxicological risk compared with many industrial residues [1,2].

At the same time, maize silage is inherently heterogeneous. Variations in dry matter (DM) and organic matter (OM) contents, the architecture of the cell-wall fractions (neutral detergent fibre (NDF), acid detergent fibre (ADF), and acid detergent lignin (ADL)), and the share of readily soluble components (sugars, organic acids, and part of the starch/oligosaccharides) can markedly alter degradation behaviour [3]. This is further shaped by the mineral profile (pH, electrical conductivity (EC), K, Na, Cl, S, as well as Ca, Mg and P) and the elemental composition, including the carbon-to-nitrogen ratio (C/N) and trace elements relevant to methanogenesis (Ni, Co, Mo, and Se) [4].

These factors influence not only methane yield expressed per unit fresh matter (FM) or volatile solids (VS) but also—critically—the kinetics of conversion. In operational practice, the time course of methane production determines safe organic loading rate (OLR), the required hydraulic retention time (HRT) [5], and buffering stability, and thus the overall economics of digester operation [6]. In this context, kinetic analysis adds information beyond BMP by indicating the speed and timing of methane release, which directly affects HRT design and short-term overload risk. Therefore, model choice is operationally relevant: the modified Gompertz model captures lag (λ) and peak rate (R_{max}), supporting start-up control and assessment of asymmetry in methane release [7]. By contrast, the first-order model provides a single rate constant (k) suitable for rapid benchmarking and for HRT planning when curves are close to mono-exponential [3,4]. Comparing both approaches helps determine whether a batch is limited mainly by hydrolysis (k) or by delayed onset/temporary inhibition (λ), leading to different decisions on blending and OLR ramp-up.

A major difficulty in describing maize silage lies in its dual character. Rapidly available fractions shape the initial phase and the production peak, whereas structural fractions—cellulose partially shielded by lignin—govern a slower and prolonged tail of conversion [8]. This pattern is further affected by environmental drivers [9]. Salinity, reflected by EC and the Na/Cl/S load, may extend the lag phase. The C/N ratio modulates the risk of ammonia-related stress. In addition, the availability of methanogenesis-related micronutrients (Ni, Co, Mo, and Se) supports enzymatic activity and process robustness. Methodologically, this means that kinetic model selection is not a cosmetic choice [4]. It is a prerequisite for the correct interpretation of BMP data and for translating laboratory outcomes into operational decisions. These include start-up strategy, progressive OLR increase, HRT selection, and blending of individual silage batches [10]. Although BMP tests are widely used to assess methane potential, their practical value increases substantially when methane accumulation curves are characterised by parameters with clear technological meaning [7].

Two empirical models are well established in the literature and in engineering practice for this substrate matrix. The modified Gompertz model represents the typical sigmoidal methane accumulation curve using three parameters with a transparent interpretation: the asymptote G_{max} (BMP per VS), the maximum methane production rate R_{max}, and

the lag phase λ [7]. The first-order model (Cone, m = 1) simplifies the description to an asymptote G_∞ and a single rate constant k, treating particulate hydrolysis as the dominant limitation [4,11]. This makes it parsimonious and estimation-stable. It is therefore useful for benchmarking series of samples, particularly when curves are close to mono-exponential (high soluble fraction, moderate lignin content, and negligible lag) [3]. The choice between these approaches should follow the study aim and the nature of the data [12].

Accordingly, the aim of this study was to evaluate the batch kinetics of AD of maize silage and to identify the most operationally informative model for describing BMP profiles, with emphasis on start-up, stepwise OLR ramp-up, and HRT selection. The scope comprised ten silage batches (A–J) spanning a realistic range of quality attributes. These included pH and EC, DM and ash, protein–lipid–fibre fractions, fibre architecture (NDF/ADF/ADL) together with derived fractions (hemicellulose, cellulose and residual OM), C/N ratio, and macro- and micronutrient profiles, with particular attention to trace elements relevant to methanogenesis (Ni, Co, Mo, and Se). BMP curves were fitted using the modified Gompertz model and a first-order model (m = 1). The resulting kinetic parameters were then mapped quantitatively onto measurable feedstock characteristics. The working hypothesis was that λ and Rmax are sensitive to salinity and the share of readily biodegradable fractions, whereas the first-order constant k reflects hydrolysis resistance governed primarily by the ADL-to-cellulose ratio. It was further assumed that model choice predictably affects operational conclusions relevant to stable and efficient renewable energy production in biogas plants.

2. Materials and Methods

2.1. Substrates and Sample Preparation

Maize silage samples were collected from 10 different clamps located on farms in the Wielkopolska region (Poland). At each site, material was taken from the working face of the silo/clamp (the surface layer exposed to oxygen was removed to a depth of approximately 20–30 cm), and a composite sample was then prepared. Immediately after collection, the material was cooled (4 °C) and transported under conditions limiting oxygen exposure. Weighed test portions were promptly directed to analyses.

Prior to loading into the reactors, each silage batch was mechanically homogenised and comminuted to a reproducible particle-size fraction to reduce the influence of particle-size heterogeneity on hydrolysis and BMP (Biochemical Methane Potential). Homogenisation and comminution were performed using a knife mill (Retsch GM 200, Retsch GmbH, Haan, Germany), maintaining consistent fraction geometry through fixed settings of processing time and rotational speed. To ensure comparability between batches (A–J), an identical sample-preparation scheme was applied (constant feed mass to the mill, constant processing time, and constant comminution speed), and the milled material was mixed to homogeneity prior to portioning. Samples were stored at 4 °C only until test preparation, and all procedures were carried out as rapidly as possible to limit secondary aerobic fermentation. The material was stored in sealed containers with an oxygen barrier (vacuum food bags/containers, Tefal, Rumilly, France) and opened immediately before portioning into the reactors.

2.2. Fermentation Conditions

Biochemical methane potential assays were conducted in stationary anaerobic reactors in accordance with German DIN/VDI guidance for biomass (historically DIN 38414-S8 and currently the widely applied VDI 4630 methodology, with adaptations to the investigated material). Fermentation was carried out in 2 L anaerobic reactors. The tests were performed in identical, sealed vessels without substrate feed, under constant temperature, and without

liquid or gas exchange other than the controlled release of biogas to the measurement system. Each experimental variant was run in triplicate, and, within each series, inoculum blanks and a positive control were included in the same number of replicates to enable result correction and validation of inoculum activity [13–15]. A schematic overview of the experimental setup is provided in Figure 1.

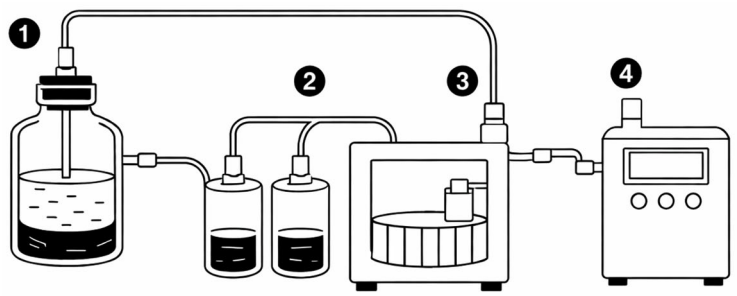

Figure 1. Schematic overview of the BMP reactor and gas measurement line (side view); 1—sealed 2 L anaerobic reactor, 2—gas-tight measurement reservoirs, 3—drum-type gas metre, and 4—portable biogas analyser (authors' own elaboration).

The reactors (1) were charged with inoculum and substrate such that the liquid phase occupied approximately 70–75% of the reactor volume, leaving headspace for gas accumulation. Laboratory-grade borosilicate glass reactors (DURAN®, DWK Life Sciences, Mainz, Germany) were used, fitted with butyl rubber stoppers and aluminium crimp seals (Sigma-Aldrich, Merck KGaA, Darmstadt, Germany). After assembly, the tightness of connections (stoppers–crimps–tubing) was checked prior to each series to eliminate the risk of measurement gas losses. Before the start of the experiment, oxygen was removed by flushing the headspace with an N_2/CO_2 mixture (80/20, *v*/*v*), after which the vessels were sealed. The gas mixture was supplied by Air Products Sp. z o.o., Warsaw, Poland. Temperature was maintained at a constant mesophilic level (39 °C). The reactors (see Figure 1) were operated without continuous mixing and with the option of gentle shaking. Temperature was ensured using a forced-air circulation incubator (Binder BD, BINDER GmbH, Tuttlingen, Germany), and rocking was provided by a rocking shaker (Edmund Bühler SM-30, Edmund Bühler GmbH, Bodelshausen, Germany) operated at low amplitude. This operating mode limited the influence of oxygen carriers, facilitated gas balancing, and minimised measurement-related contamination.

The inoculum consisted of stable digestate from an operating anaerobic installation. Prior to the test, the inoculum was pre-incubated for 3–7 days at the test temperature, without substrate addition, until daily biogas production decreased to background levels. The dry matter (DM) and volatile solids or organic dry matter (VS) contents of the inoculum were determined using gravimetric procedures, analogously to the substrate. Pre-incubation enabled stabilisation of the methanogenic background and reduced the influence of residual inoculum biodegradability on BMP curve profiles. The substrate-to-inoculum ratio (ISR) was set at 0.3 g VS_substrate per g VS_inoculum to avoid acidification and ammonium inhibition. The doses were calculated based on the measured VS contents of both components.

The test duration was defined until production stabilisation was achieved and daily production declined to a background level, ensuring closure of BMP curves and the correctness of kinetic parameter estimation. The stabilisation criterion was taken as a decrease in daily production to the inoculum blank level and maintenance of this condition over subsequent days, which limited the risk of underestimating the BMP asymptote. Daily biogas production was determined from volume readings using calibrated, gas-tight measurement reservoirs (2) connected to the reactors (1) via tubing (see Figure 1) and was recorded using

a drum-type gas metre (3) (Ritter Drum-type Gas Meter, Ritter Apparatebau GmbH & Co. KG, Bochum, Germany). Biogas composition (CH_4, CO_2, O_2, and H_2S in control mode) was determined using a portable biogas analyser (4), Geotech GA5000 (Geotech, Coventry, UK), serviced and verified by the distributor Tusnovics Instruments Sp. z o.o. (Kraków, Poland). Measurements were performed in accordance with the manufacturer's instructions, after stabilisation of analyser readings for the gas sample from a given reactor. CH_4 and CO_2 were measured by non-dispersive infrared (NDIR) absorption, while O_2 was measured using an electrochemical sensor, in line with the device specification. The analyser was calibrated with reference gases prior to each series and periodically during the experiments. Calibration gases were supplied by Air Products and Chemicals Inc. (Allentown, PA, USA). Calibration was performed using at least a two-point (zero/span) procedure, in accordance with the instrument protocol, and the reference gas had a certified composition.

2.3. Physicochemical Analysis of Maize Silage

2.3.1. pH Measurement

Measurements were carried out using a calibrated pH metre, following the requirements of ISO 10523:2008 [16]. Prior to measurement, each sample was thoroughly mixed, and the electrodes were calibrated using fresh buffer solutions (pH 4.00 and pH 7.00). Measurements were performed at room temperature (~20 °C) for all samples, using an identical procedure throughout. A multi-parameter metre with a combined pH electrode was used (WTW Multi 3630 IDS, Xylem Analytics Germany GmbH, Weilheim, Germany).

2.3.2. Dry Matter Content

In accordance with ISO 11465:1993 (adapted for plant material), dry matter was determined gravimetrically by drying to constant mass at 105 °C. The crucibles/dishes were pre-dried at 105 °C, cooled in a desiccator, and weighed prior to analysis [17]. A weighed portion of silage (typically 3–10 g fresh mass) was dried at 105 °C for ~24 h with forced air circulation; after cooling, it was weighed and, if necessary, re-dried (mass change < 0.1%). The result was calculated as the fraction of mass after drying relative to fresh sample mass, accounting for tare. To reduce variability, a thin material layer was used in the vessel and consistent preparation conditions were maintained. Drying was performed in a forced-air laboratory oven (Memmert UN, Memmert GmbH + Co. KG, Schwabach, Germany), and weighing was carried out using an analytical balance (RADWAG, Radom, Poland).

2.3.3. Organic Dry Matter and Ash Content

Organic matter was determined by loss on ignition in a muffle furnace: after dry matter determination, 1–3 g of dried sample was weighed into pre-ignited crucibles and ashed at 550 °C for 5 h. After cooling in a desiccator, crucibles were weighed; if required, ashing was continued to constant mass. Ash in DM (%) was calculated as the fraction of inorganic residue in dry mass, and organic dry matter in DM (%) = 100 − ash. Organic dry matter in fresh mass was calculated by multiplying by the DM fraction. Duplicates and an empty crucible were included in each series [15]. Ashing was performed in a muffle furnace (Nabertherm L, Nabertherm GmbH, Lilienthal, Germany).

2.3.4. Electrical Conductivity

Electrical conductivity, used as an indicator of the concentration of dissolved electrolytes, was measured with a calibrated conductivity metre in accordance with ISO 7888:1985 [18]. Silage samples were mixed in a measured volume of deionised water. Prior to the measurement series, the cell constant was calibrated, and readings were checked using standard solutions. Measurements were performed at room temperature

with compensation to 25 °C. After stabilisation of the reading, the result was recorded as specific conductivity (mS/cm). EC was measured using a conductivity probe with automatic temperature compensation (WTW TetraCon® 925, Xylem Analytics Germany GmbH, Weilheim, Germany) coupled with the WTW Multi 3630 IDS metre. To limit the effect of phase ratio and ion extraction, a fixed, reproducible sample mass-to-deionised water volume ratio was applied throughout the series.

2.3.5. Micro- and Macroelement Content

Macroelements (Ca, P, K, Mg, Na, S, and Cl) and micro/trace elements (Fe, Zn, Cu, Mn, Co, Se, Mo, and Ni) were determined in maize silage on a dry matter basis. The sample was homogenised, then dried to constant mass, and 0.25–0.50 g of dried sample was weighed into PTFE vessels. For chlorides, an aqueous extract was prepared to limit losses during acid digestion. For trace elements such as Co, Se, Mo and Ni, ICP-MS was used, while ICP-OES was applied for the remaining micro- and macroelements, with appropriate selection of emission lines and background correction. In each analytical series, a reagent blank, a reference material (if available), and a calibration verification standard were included to confirm signal stability and analytical correctness. Sample preparation for ICP was conducted using microwave digestion (ETHOS One, Milestone Srl, Sorisole, Italy) in PTFE vessels; ICP-OES measurements were performed using a spectrometer (Thermo iCAP Dual 6500, Thermo Fisher Scientific, Bremen, Germany), whereas ICP-MS measurements were carried out using a spectrometer (Agilent 7900 ICP-MS, Agilent Technologies, Santa Clara, CA, USA).

2.3.6. Crude Protein and Total Nitrogen

Crude protein (CP) was expressed as total nitrogen content multiplied by 6.25, referenced to dry matter (DM). The factor 6.25 assumes an average nitrogen content of 16% in proteins (100/16= 6.25).

Total nitrogen (N-total) was determined using the Kjeldahl method in accordance with ISO 5983-2:2009 and AOAC Official Method 2001.11 (feed matrices; block digestion/steam distillation) [19]. Sample digestion in concentrated H_2SO_4 in the presence of a catalyst (K_2SO_4/$CuSO_4$ or TiO_2), conversion of N to $(NH_4)_2SO_4$ → alkalisation → distillation of ammonia into a receiving solution (boric acid) → titration (HCl/H_2SO_4). Digestion and distillation were performed using an automated Kjeldahl system (Kjeltec™ 8400, FOSS, Hillerød, Denmark), and titration was conducted automatically within the distillation unit.

2.3.7. Crude Lipids

Crude lipid content (CL) in maize silage was determined by acid hydrolysis, followed by solvent extraction (Weibull–Stoldt procedure), in accordance with ISO 6492:1999 [20]. The result was expressed as % of lipid extract mass on a dry matter basis. Acid hydrolysis was performed by heating the sample with 3–4 mol/L HCl (approx. 100 mL) for 30–60 min under reflux to loosen the matrix and release fat from protein–fibre complexes. The residue was filtered through ashless filter paper and rinsed with hot water to neutral pH. The residue together with the filter was dried at 100–105 °C to constant mass. The dried residue was extracted with petroleum ether. Extraction was carried out using a Soxhlet apparatus (Soxtherm® 2000, C. Gerhardt GmbH & Co. KG, Königswinter, Germany).

2.3.8. Crude Fibre

Crude fibre (CF) was determined by sequential acid and alkaline digestion with ash correction (Weende crude fibre), following ISO 6865:2000 and AOAC Official Method 962.09 (feed matrices) [21]. The result was expressed as % of the fibre fraction mass on a dry matter basis (DM). The CF method is complementary to the Van Soest system

(NDF/ADF/ADL) but differs in operational definition. CF was determined using a fibre analysis unit (Fibretherm® FT12, C. Gerhardt GmbH & Co. KG, Königswinter, Germany).

2.3.9. Determination of Detergent Fibre Fractions

To avoid terminological ambiguity throughout the manuscript, NDF/ADF/ADL are reported as detergent fibre fractions, and ash-corrected variants (aNDFom, ADFom, and ADLom) were used for derived fraction calculations [22].

NDF (Neutral Detergent Fibre) was defined as the cell-wall fraction resistant to neutral detergent solution; operationally, it corresponds to the sum of hemicellulose, cellulose and lignin after ash correction. The silage sample was homogenised, and its dry matter content was determined by drying at 105 °C to constant mass, so that all results could be reported as % DM. Where fat content was elevated, preliminary defatting with petroleum ether was applied. Approximately 0.5–1.0 g of material (on a DM basis) was treated with neutral detergent solution according to the Van Soest system, with addition of thermostable α-amylase to remove starch and, optionally, Na_2SO_3 to disrupt protein–lignin complexes. The suspension was heated to boiling under reflux for approximately 60 min, maintaining constant boiling intensity and mixing. The hot suspension was then filtered through Gooch crucibles with a celite layer, after which the residue was thoroughly rinsed with hot water and then with acetone to remove soluble components and accelerate drying. The residue was dried at 105 °C to constant mass and weighed; subsequently, the same filter/bag was ashed at 550 °C for 2 h, cooled in a desiccator, and weighed again. Ash-corrected NDF (aNDFom) was calculated as the difference between residue mass after drying and after ashing, corrected for the celite blank, relative to sample mass on a dry matter basis, and expressed as %. NDF/ADF analyses were performed using a reflux-based fibre analyser (Fibertec™ 8000, FOSS, Hillerød, Denmark), according to the Van Soest system; Gooch crucibles and filtration materials were selected as components compatible with the system filtration configuration.

ADF (Acid Detergent Fibre) was determined within the Van Soest system as the cell-wall fraction resistant to acid detergent solution, operationally corresponding to the sum of cellulose and lignin after ash correction. The silage sample was homogenised; where fat content was elevated, preliminary defatting with petroleum ether was applied. Approximately 0.5–1.0 g of material (on a DM basis) was heated to boiling in ADF solution (typically CTAB in 1 N H_2SO_4) for approximately 60 min under constant boiling intensity and mixing, after which the hot suspension was filtered through Gooch crucibles with a celite layer. The residue was thoroughly rinsed with hot water to remove the reagent, and then with acetone to eliminate soluble components and accelerate drying; the material was dried at 105 °C to constant mass and weighed, and then the same filter was ashed at 550 °C for 2 h, cooled in a desiccator, and weighed again. Ash-corrected ADF was calculated as: (mass of ADF residue after drying-ash mass of the same residue), corrected for the celite blank, relative to sample mass on a dry matter basis, and expressed as %.

ADL (Acid Detergent Lignin) was determined within the Van Soest system as the portion of the ADF fraction insoluble in concentrated sulphuric acid; operationally, it corresponds to detergent lignin after ash correction. Where fat content was elevated, preliminary defatting with petroleum ether was applied. After ADF determination, the same residue (in Gooch crucibles with a celite layer) was treated with 72% H_2SO_4 at room temperature, maintaining a fixed solid-to-acid ratio of ~1:10 (m/m) and intensive, periodic mixing for approximately 3 h to ensure full reagent–matrix contact. After digestion, the suspension was cautiously diluted with distilled water to a concentration of ~3 N, filtered, and the residue was rinsed with hot water to neutral pH and then with acetone (enabling removal of residual solubles and faster drying). The material was dried at 105 °C to constant

mass and weighed; subsequently, the same filter was ashed at 550 °C for 2 h, cooled in a desiccator, and weighed again. ADL content in % DM (om variant—ash corrected) was calculated as the difference between residue mass after drying and after ashing, corrected for the celite blank, relative to sample mass on a dry matter basis, and expressed as %.

2.4. Determination of Derived Fractions: Hemicellulose, Cellulose and Residual OM

Derived fractions were calculated on a dry matter basis using the Van Soest system, determined in the ash-corrected variant (aNDFom, ADFom, and ADLom), to avoid overestimation associated with residual ash. Hemicellulose was operationally defined as the difference between neutral and acid detergent fibre, corresponding to the portion of the cell wall soluble in acid detergent solution but insoluble in neutral detergent. Computationally, hemicellulose was calculated as aNDFom-ADFom. Cellulose was calculated as the difference between the acid detergent fraction and detergent lignin, representing, approximately, the cellulose polymer remaining after subtracting ADL.

Residual organic matter was determined by closing the organic matter balance; subsequently, the residual OM value was interpreted as the fraction not classified as cell-wall material and CP/CL macronutrients (including soluble sugars, pectins, part of starch/oligosaccharides after amylase action, organic acids, and extracts), and in calculations, it was constrained to non-negative values within uncertainty limits [23]. To avoid propagation of computational errors, all derived fractions were consistently determined on the same basis (DM, ash-corrected variant), and results were reported using a consistent unit (% DM).

For clarity, Table 1 summarises how hemicellulose, cellulose and residual organic matter were derived from the ash-corrected detergent fibre fractions (aNDFom, ADFom and ADLom) on a dry matter basis.

Table 1. Derivation of hemicellulose, cellulose and residual organic matter from ash-corrected detergent fibre fractions (basis: % DM).

Quantity	Symbol (Ash-Corrected)	Type	Calculation/Definition (Basis: % DM)
Neutral detergent fibre	aNDFom	measured	Van Soest fraction (ash-corrected)
Acid detergent fibre	ADFom	measured	Van Soest fraction (ash-corrected)
Acid detergent lignin	ADLom	measured	Van Soest fraction (ash-corrected)
Hemicellulose	Hemi	derived	Hemi = aNDFom − ADFom
Cellulose	Cell	derived	Cell = ADFom − ADLom
Residual organic matter	Residual OM	derived	Residual OM = OM − (Hemi + Cell + ADLom + CP + CL) *

* Explanations: OM denotes organic matter on a dry matter basis (% DM). CP and CL denote the macronutrient fractions reported in this study (raw protein and raw lipid, respectively). Residual OM represents the remaining organic fraction not classified as cell-wall material or CP/CL and was constrained to non-negative values within uncertainty limits.

2.5. Determination of N, C and C/N

Nitrogen content in dry matter was taken as the primary value from total nitrogen determination (Kjeldahl method); subsequently, a standard conversion factor of 6.25 (16% N in protein) was applied. Carbon content in dry matter was estimated using a component model based on the shares of fractions in % DM and their typical carbon shares in the fractions determined above, and an approximate molar C/N ratio was calculated on

this basis [15]. Uniform component-model assumptions were applied across the entire series to maintain comparability between silage batches. To ensure comparability between batches, C/N was consistently calculated on a molar rather than mass basis, using the same component-model assumptions throughout the series.

2.6. Processing of BMP Results and Calculation Corrections

BMP results were corrected for inoculum background (blank reactors) by subtracting cumulative methane production in blanks from the values obtained for reactors containing substrate. Gas volumes were converted to normal conditions (0 °C, 101.325 kPa), accounting for process temperature and atmospheric pressure. Methane yield was reported per fresh matter (FM) and per volatile solids (VS), using the DM and VS values determined for both substrate and inoculum [23]. Normalisation corrections were applied consistently for all reactors and time points within a given series. Balance calculations, unit conversions and series summaries were performed in a spreadsheet (Microsoft Excel 365, Microsoft Corporation, Redmond, WA, USA).

2.7. Kinetic Modelling of BMP Curves

Cumulative methane production curves (0–50 d) were fitted using two complementary empirical models: (i) the modified Gompertz model (Equation (1)) [7] and (ii) a first-order kinetic model in the Cone form with m = 1 (Equation (2)) [24]. The characteristic half-conversion time was derived from the first-order rate constant using Equation (3) [4].

Modified Gompertz model:

$$G(t) = G_{max}\exp\left\{-\exp\left[\frac{R_{max}e}{G_{max}}(\lambda - t) + 1\right]\right\} \quad (1)$$

where:

- G(t) is the cumulative methane yield at time t (m^3 CH_4/Mg VS),
- G_{max} is the asymptotic BMP/VS (m_3 CH_4/Mg VS),
- R_{max} is the maximum methane production rate (m^3 CH_4/Mg VS d),
- λ is the lag time (induction time) (d),
- e is the base of the natural logarithm (Euler's number; e ≈ 2.71828),
- t is the fermentation time (d).

First-order kinetic model, Cone form with m = 1:

$$G(t) = B_0\left(1 - e^{-kt}\right) \quad (2)$$

where:

- G(t) is the cumulative methane yield at time t (m^3 CH_4/Mg VS),
- B_0 is the asymptotic methane potential on a VS basis (m^3 CH_4/Mg VS),
- k is the effective first-order hydrolysis/biodegradation rate constant (d^{-1}).

Half-conversion time:

$$t_{50} = \frac{\ln 2}{k} \quad (3)$$

where:

- t_{50} is the time required to reach 50% of the asymptotic methane potential (d),
- ln 2 is the natural logarithm of 2,
- k is the first-order rate constant (d^{-1}).

Model parameters were estimated by nonlinear least-squares regression in OriginPro (OriginLab Corporation, Northampton, MA, USA; Origin 2025, v10.2) using the built-in Nonlinear Curve Fit (NLFit) tool. Parameter estimation minimised the sum of squared

residuals (SSE) between experimental and model-predicted cumulative methane yields, with the Levenberg–Marquardt algorithm used for iteration (default for explicit nonlinear fits). Fit quality was assessed using R^2 and RMSE, and the resulting kinetic parameters were subsequently interpreted in relation to analytically determined substrate characteristics.

2.8. Experimental Design and Data Analysis

This study followed a comparative design based on ten maize silage batches (A–J), representing natural variability in fractional composition. All BMP assays were conducted under identical conditions to ensure direct comparability between substrates. Each experimental variant was performed in triplicate, and the results are reported together with their associated uncertainty, as provided by the replication and measurement procedure and presented in the tables. The interpretation focuses on effect magnitudes and model-based kinetic descriptors rather than formal hypothesis testing between batches. Relationships between routine silage quality indicators and kinetic parameters were evaluated using descriptive trend analysis and regression- or correlation-based interpretation. Model performance was assessed using goodness-of-fit diagnostics obtained from nonlinear least-squares fitting, including R^2 and RMSE.

3. Results

3.1. Basic Physicochemical Characterisation of Maize Silage Samples

In the analysed set of maize silages (samples A–J, see Table 2), the acidity was typical of properly ensiled material. pH ranged from 3.76 to 4.23, with a mean of 3.98 and an uncertainty of a single determination of about ±0.13–0.15. From the perspective of AD operation, such values are desirable, as they indicate lactic-acid dominance and effective microbiological stabilisation. Moreover, the acidity of the feedstock does not constitute a process limitation once diluted in the digester volume and in the presence of bicarbonate buffering from digestate [25]. During feedstock preparation, each batch should be briefly conditioned in a feed tank with recirculated digestate rather than adjusted by direct addition of alkaline reagents. This approach shortens the lag and stabilises conditions for methanogens without generating additional salts [26].

Table 2. pH and electrical conductivity (EC) results for maize silage samples.

Sample	pH	Uncertainty (+/−)	Electrical Conductivity (mS/cm)	Uncertainty (+/−)
A	3.9	0.14	6.4	0.20
B	4.0	0.14	**4.2**	0.13
C	4.0	0.14	5.4	0.17
D	4.1	0.14	9.2	0.29
E	3.9	0.14	8.3	0.26
F	**4.2**	0.15	6.8	0.22
G	4.0	0.14	9.3	0.29
H	3.9	0.14	8.9	0.28
I	**3.7**	0.13	7.1	0.23
J	3.8	0.13	**10.3**	0.32

Explanation: minimum and maximum values are shown in bold to support comparison.

The electrical conductivity of the aqueous extracts (4.29–10.30 mS/cm, mean 7.65 mS/cm, with an uncertainty of a single measurement of ±0.20–0.32 mS/cm, see

Table 2) indicates variable electrolyte loads. The dominant ions are likely potassium, sodium and chloride, with possible contributions from ammonium and sulphates. Elevated EC in several batches (notably D, G, H and J) is not synonymous with toxicity. It indicates a need for controlled feeding. These batches should be introduced gradually and blended with lower-EC batches such as B and C. Where needed, the ionic profile should be confirmed by rapid determination of K, Na and Cl (ICP or IC) in operational material [27].

Importantly, pH and EC in this dataset are only weakly related. Acidity primarily reflects volatile organic acids. Conductivity mainly represents the mineral salt load. Therefore, the two indicators should be interpreted independently. pH should be used as a measure of silage maturity and stability. EC should be used as an indicator of osmotic risk in the digester.

The pH and EC profiles are favourable for AD. Under standard mesophilic conditions and alkalinity 3–5 g $CaCO_3$/L, these batches should not trigger acidification or osmotic shocks [25]. A simple batch-management procedure is recommended. Batches should be pre-conditioned with recirculated digestate, raising the feeding mixture pH to 6.2–6.8. The organic loading rate should be controlled when introducing the highest-EC batches. Key process indicators should be monitored routinely (TAN/NH_4^+, conductivity of the liquid phase, FOS/TAC). Kinetics will depend on NDF, ADF, ADL and BMP expressed per VS. Already in Table 2, the silages show a profile consistent with stable methanogenesis, while the highest-EC batches require only basic caution and, where appropriate, confirmation of the ionic profile [28].

In the studied set of maize silages (A–J, see Table 3), dry matter content ranged from 28.7 to 35.3% (mean 31.9%). This range supports stable AD and convenient handling [29]. The two batches with the lowest DM (C: 28.7% and G: 29.3%) may be more prone to effluent losses and faster release of VFAs. The highest value (D: 35.3%) supports a higher energy load per unit fresh mass. At the same time, the share of organic matter in dry matter (OM/DM) remained high and relatively uniform, at 90.1–95.5% (mean 92.7%). Particularly high values were observed for I (95.5%), C (94.9%) and B (94.4%). Ash content ranged from 4.5 to 9.9% (mean 7.3%). Elevated values for A (9.9%) and F (9.2%) suggest mineral admixture, such as soil contamination during harvest, and a potential dilution of the energetic value of the feedstock. In view of the declared uncertainties (typically ±1.05–1.29 percentage points for DM, ±3.5–3.7 percentage points for OM, and ±1.65–3.63 percentage points for ash), differences of 1–2 percentage points between samples may not be statistically meaningful. Multi-point contrasts are more informative, such as A (OM 90.1%) versus I (95.5%).

From an energetic and mass-balance perspective, the DM–OM combination indicates an expected methane yield on a fresh-mass basis typical of good-quality silage. For mean dataset parameters (DM 31.9% and OM/DM 92.7%), the volatile solids fraction in fresh mass is approximately $0.319 \times 0.927 \approx 0.295$ kg VS/kg FM. With BMP–VS around 0.35–0.38 m^3 CH_4/kg VS, this corresponds to ~0.103–0.112 m^3 CH_4/kg FM. This matches the reported 0.10–0.12 m^3 CH_4/kg FM [30,31]. Accordingly, the highest potential per FM is expected for batches combining elevated DM with high OM (e.g., B: 33.6%/94.4%, D: 35.3%/91.8%, H: 33.7%/91.9%, and J: 31.8%/93.7%). Batches with lower DM (C and G) or higher ash (A and F) are best blended to homogenise the energy load and reduce OLR fluctuations.

It should be noted that higher ash, beyond lowering the organic matter share, may increase the ionic load (K^+, Na^+, and Cl^-) in the digester liquor. This does not in itself disqualify the feedstock. It supports routine mineral screening and cautious feeding during initial introduction. Overall, the DM, OM and ash profiles of the analysed silages can be assessed as highly favourable for AD. Under standard alkalinity buffering and appropriate mixing, feeding these batches should result in stable methanogenesis and yields consistent with estimates derived from the parameters presented [32].

Table 3. Basic physicochemical characteristics of maize silage samples.

Sample	Dry Matter (%)	Uncertainty (+/−)	Organic Matter [%]	Uncertainty (+/−)	Ash (%)	Uncertainty (+/−)
A	32.2	1.18	90.1	3.47	**9.9**	3.63
B	33.6	1.23	94.4	3.64	5.6	2.05
C	**28.7**	1.05	94.9	3.66	5.1	1.87
D	**35.3**	1.29	91.8	3.54	8.2	3.01
E	31.1	1.14	91.5	3.53	8.5	3.12
F	32.6	1.19	**90.8**	3.50	9.2	3.37
G	29.3	1.07	92.8	3.58	7.2	2.64
H	33.7	1.23	91.9	3.54	8.1	2.97
I	30.3	1.11	**95.5**	3.68	**4.5**	1.65
J	31.8	1.16	93.7	3.61	6.3	2.31

Explanation: minimum and maximum values are shown in bold to support comparison.

The pH range indicates well-preserved silage and low risk of acidification under standard AD conditions. High-EC batches require gradual introduction and blending, with rapid ion checks when needed. DM, OM and ash values support stable operation, while high-ash batches merit mineral screening.

3.2. Results of BMP Tests: Biogas and Methane Yields

The results in Section 3.1 indicate that the analysed maize silages were properly preserved and had a favourable DM and VS profile. This profile is relevant for handling and methane performance. These observations were verified using BMP tests, which are treated here as direct indicators of conversion efficiency. To separate moisture effects from organic matter quality, results are reported on a fresh matter basis and normalised to DM and VS (see Table 4).

Table 4. Biogas and BMP results for the analysed maize silages.

Sample	Biogas (m^3/Mg FM)	Unc. (+/−)	BMP (m^3 CH_4/Mg FM)	Unc. (+/−)	BMP (m^3 CH_4/Mg DM)	Unc. (+/−)	BMP (m^3 CH_4/Mg VS)	Unc. (+/−)
A	189.1	7.40	102.1	4.21	317.0	13.42	351.8	15.17
B	209.3	8.20	117.0	4.83	348.3	14.75	369.0	15.91
C	191.3	7.49	105.1	4.33	366.0	15.50	385.7	16.63
D	**211.9**	8.30	**120.3**	4.96	340.7	14.43	371.1	16.00
E	204.8	8.02	114.2	4.71	**367.3**	15.56	**401.5**	17.31
F	**189.2**	7.40	102.1	4.21	**313.1**	13.26	344.8	14.86
G	189.6	7.42	104.0	4.29	354.8	15.03	382.3	16.48
H	205.5	8.05	114.8	4.74	340.7	14.43	370.7	15.98
I	195.4	7.65	107.3	4.42	354.0	14.99	370.6	15.98
J	189.8	7.43	**100.2**	4.13	315.0	13.34	**336.2**	14.49

Explanations: FM—fresh matter, DM—dry matter, VS—volatile solids, Unc.—uncertainty; minimum and maximum values are shown in bold to support comparison.

Table 4 presents the BMP results. Biogas production on a fresh matter basis ranged from 189 to 212 m^3/Mg FM, and the corresponding methane yield was 100–120 m^3 CH_4/Mg FM. Both values are consistent with expectations for maize silage with a dry matter content

of ~29–35% and an organic matter share in DM of ~90–95%. Fresh-matter yields are primarily driven by DM and VS per unit fresh mass (Table 3). Higher DM results in higher biogas and methane volumes per tonne of fresh feedstock. For instance, sample D (DM 35.3%, VS/DM 91.8%) achieved the highest FM-based BMP of 120.3 m^3 CH_4/Mg FM and 211.9 m^3/Mg FM of biogas. The BMP to biogas ratio of ≈0.567 implies a methane content of ~57%. This value falls within the typical range of 53–57% reported for this matrix. A similar pattern was observed for B, E and H (DM 31.8–33.7%). These samples ranked highest in FM-based BMP (114–117 m^3 CH_4/Mg FM). In contrast, C and G, with slightly lower DM (28.7–29.3%), showed only moderate FM-based yields despite high organic quality. This confirms that water dilution limits yields expressed per tonne of fresh matter [33,34].

Normalisation to DM and VS separates the effect of moisture from the quality of biodegradable matter. BMP on a DM basis ranged from 313 to 367 m^3 CH_4/Mg DM, while BMP on a VS basis ranged from 336 to 402 m^3 CH_4/Mg VS. The highest VS-based BMP was observed for E (401.5), C (385.7) and G (382.3). These batches had high VS/DM (≥91.5%) and low ash (≤8.5%), consistent with Table 3. Conversely, A (351.8) and F (344.8) showed the lowest BMP on a VS basis and the highest ash contents (9.9% and 9.2% DM). This pattern indicates a higher mineral fraction and a smaller biodegradable fraction. It reduces yields after normalisation to DM and VS. Sample J had the lowest BMP on a VS basis (336.2) despite moderate DM (31.8%) and a good VS/DM share (93.7%). In Table 2, this sample also showed the highest electrical conductivity (10.3 mS/cm). This may indicate a higher salt load. While this does not imply toxicity on its own, it can mark batches with a less favourable structural profile and or a higher share of more slowly hydrolysable material. Therefore, in practice, such batches should be blended with other substrates and introduced gradually [35,36]. Uncertainties were similar across the dataset, at about 3.5–4.5% for all four metrics. They do not change the ranking. Differences of several to more than ten m^3 CH_4/Mg are operationally meaningful. Differences of 2–4 m^3 may fall within measurement error.

Overall, the results in Table 4 confirm good methane production performance of the analysed silages. On a fresh matter basis, the highest yields are expected for batches with higher DM (D, B, E, and H). On a VS basis, E, C and G performed best. In conjunction with Table 2, only basic operational caution is needed for batches with high EC (D, G, H, and J). Blending and controlled OLR are recommended. Batches with higher ash (A and F) should be treated as feedstocks with lower fuel value per unit mass. From an operational perspective, this profile is predictable and favourable. Under standard buffering and appropriate substrate management, these batches should support stable methanogenesis. The yields in Table 4 match expectations based on DM, VS and the physicochemical parameters presented earlier.

Fresh-matter yields track DM content, so higher-DM batches provide more methane per tonne of feedstock. VS-based BMP highlights organic quality, where E, C and G perform best. High EC or ash calls for blending and controlled feeding, but the overall profile supports stable methanogenesis.

3.3. Chemical Composition and Analytical Fractions of Maize Silage Versus BMP Variability

The BMP results (Table 4) show that biogas and methane yields differed among the analysed batches (A–J), despite the generally favourable physicochemical profile (Tables 2 and 3). Therefore, the next step was to assess whether the observed BMP variability can be explained by the basic chemical composition of the silages. This assessment focused on CP, CL and CF (see Table 5).

Table 5. Profile of the main chemical fractions of the analysed maize silage samples.

Sample	CP % DM	Uncertainty (+/−)	CL % DM	Uncertainty (+/−)	CF % DM	Uncertainty (+/−)
A	**11.1**	0.26	2.7	0.07	18.3	0.52
B	7.3	0.17	3.4	0.09	23.9	0.68
C	9.4	0.22	3.9	0.10	**24.9**	0.71
D	6.7	0.16	**4.5**	0.12	**18.1**	0.52
E	**6.5**	0.15	2.6	0.07	23.0	0.66
F	9.0	0.21	3.7	0.10	20.9	0.60
G	7.7	0.18	2.9	0.08	24.3	0.69
H	8.8	0.21	**2.5**	0.07	18.1	0.52
I	7.3	0.17	3.7	0.10	19.2	0.55
J	8.6	0.20	2.8	0.07	21.6	0.62

Explanations: CP—crude protein, CL—crude lipid, CF—crude fibre; minimum and maximum values are shown in bold to support comparison.

In light of Table 5, the profile of the main chemical fractions of maize silage (CP, CL and CF, all expressed as % DM) helps to explain the variability reported earlier in Tables 2–4. It also supports a more targeted interpretation of substrate behaviour during anaerobic digestion [37,38]. Crude protein ranged from 6.5 to 11.1% DM and, assuming the standard conversion CP ≈ 6.25·N, indicates a moderate nitrogen load typical of maize. Batches with higher CP (A: 11.1%, H: 8.8%, and F: 9.0%) may show a lower molar C/N ratio and a greater tendency towards TAN and NH_4^+ accumulation under excessive OLR. At the same time, CP contributes buffering capacity and may shorten the initial phase of methanogenesis. This pattern is consistent with Table 4. Sample A, despite the highest ash content (Table 3) and average DM, maintained an acceptable BMP/VS, yet did not stand out on an FM basis. This suggests that higher CP did not offset mineral and moisture dilution [39]. The opposite tendency is evident for D (CP 6.7%). A lower nitrogen load reduces the risk of ammonia-related effects and, combined with elevated DM (35.3%), supports higher yields on an FM basis, as reflected in Table 4.

Crude lipid content (CL 2.5–4.5% DM) remained within a safe range for AD and is favourable in terms of energy contribution. It does not approach inhibition linked to long-chain fatty acids. In practice, this means that batches with higher CL (D: 4.5%, C and I: 3.7–3.9%) may slightly increase methane share in biogas and shorten lag, provided that syntrophic β-oxidation remains efficient [40]. This trend aligns well with Table 4. D, E and H achieved high BMP on an FM basis, while C, despite lower DM, compensated through organic quality (BMP/VS in the upper part of the distribution). Importantly, CL levels of 2.5–4.5% do not require any specific operational measures beyond stable feeding and ensuring adequate availability of trace elements (Ni, Co, and Se).

The most pronounced kinetic signal is associated with CF (18.1–24.9% DM). CF primarily affects the hydrolysis rate and subsequent conversion to methane. Batches with higher CF (B: 23.9%, C: 24.9%, G: 24.3%, and E: 23.0%) are likely to release structural carbohydrates more slowly and to depend more strongly on fibre quality (NDF, ADF and ADL). This helps to explain differences in BMP/VS among samples with similar DM. High CF does not necessarily reduce yield if ADL remains moderate (detergent fibre table). However, a higher lignin share is a clear constraint [41]. In the present dataset, E and C, despite CF ≥ 23%, ranked among the leaders in BMP/VS (Table 4). This points to a more favourable fibre structure, such as lower lignin share or higher hydrolytic accessibility. In contrast, H and D

(CF 18.1%) combined a lower fibre load with higher DM. This supports higher FM-based yields and may improve start-up kinetics. A further link with Table 2 should be noted. Batches with high electrical conductivity (D, G, H, and J) may carry a higher salt load. If this coincides with high CF and elevated ADL, hydrolysis may slow down. In such cases, blending with lower-EC materials, such as B and C, and maintaining alkalinity at 3–5 g $CaCO_3$/L support process stability.

From an operational perspective, the CP, CL and CF profiles in Table 5 support three practical conclusions based on the dataset as a whole. First, for batches with higher CP (A, F, and H), maintaining a moderate ISR and controlling TAN during start-up is advisable. The expected benefit is good microbial activity and a shorter lag [42,43]. Second, CL levels across the series are safe and may support methane yields. Dose reduction is not required, provided that OLR is kept stable and digestate recirculation is effective [44]. Third, CF, together with DM and VS (Table 3) and pH and EC (Table 2), will determine whether supportive measures are needed. These may include size reduction, supplementation with cellulolytic and hemicellulolytic enzymes, or extending HRT during operation on the most fibre-rich batches [45,46]. Overall, Table 5 completes the picture. The analysed maize silages are predictable substrates with stable AD performance. Their behaviour can be fine-tuned by batch blending based on DM and VS (Table 3), pH and EC (Table 2), and BMP targets on an FM and VS basis (Table 4).

The BMP variability is consistent with shifts in CP, CL and CF across the batches. Higher CP can support buffering but increases TAN risk under high OLR. Higher CF can slow hydrolysis, so fibre quality becomes decisive for VS-based BMP. The overall profile supports stable AD when batches are blended and feeding remains controlled.

3.4. Detergent Fibre Profile (NDF/ADF/ADL)

The detergent fibre profile presented in Table 6 provides a clear description of the quality of the analysed maize silages and helps to explain the differences in their behaviour during anaerobic digestion observed in the preceding tables. The NDF content ranged from 39.6 to 51.2% DM, ADF from 26.6 to 35.2% DM, and ADL from 3.7 to 7.4% DM. The associated uncertainties were relatively low (approximately ±1.1–1.5, ±0.8–1.0, and ±0.10–0.21 percentage points, respectively), so the between-sample differences can be considered relevant from a process perspective. Functionally, NDF reflects the overall cell-wall load and provides substrate for hydrolysis. ADF represents the more recalcitrant portion and includes cellulose and lignin. ADL indicates the kinetic barrier and reflects the detergent lignin share. An increase in ADL typically slows hydrolysis and reduces the expected rate of methanogenesis [47].

Simple derived relationships (Hemicellulose ≈ NDF − ADF, Cellulose ≈ ADF − ADL) indicate two distinct material types. Silages with high NDF but moderate ADL, such as H (NDF 51.2%, ADF 34.0%, and ADL 4.7% DM), carry a substantial fibre load, yet show a favourable structure. They have high cellulose of ~29.3% DM and relatively low lignin. This supports good conversion when HRT is adequate. This is consistent with Table 4, where H maintained high yields on an FM basis (biogas 205.5 m^3/Mg FM, BMP 114.8 m^3 CH_4/Mg FM). This performance is also supported by a solid DM level (33.7%) in Table 3 and a favourable macronutrient profile (Table 5, CF 18.1% DM). By contrast, silages with higher ADF and elevated ADL, such as G (NDF 46.5%, ADF 35.2%, and ADL 7.3% DM) or D (NDF 49.4%, ADF 31.8%, and ADL 7.4% DM), indicate a more resistant fibre structure. In practice, this implies a slower hydrolysis phase and greater sensitivity to overly aggressive OLR [48]. Importantly, ADL affects the rate more strongly than the ultimate yield. In the BMP tests (Table 4), sample G achieved a high BMP/VS (382.3 m^3 CH_4/Mg VS). This suggests that,

with sufficiently long incubation and an active inoculum, the lignin constraint reduces mainly the pace rather than the overall potential [49].

Table 6. Detergent fibre profile of the analysed maize silages.

Sample	NDF % DM	Uncertainty (+/−)	ADF % DM	Uncertainty (+/−)	ADL % DM	Uncertainty (+/−)
A	48.8	1.40	**26.6**	0.76	6.0	0.17
B	46.9	1.34	31.3	0.90	7.3	0.21
C	45.1	1.29	29.0	0.83	4.7	0.13
D	49.4	1.42	31.8	0.91	**7.4**	0.21
E	42.3	1.21	31.4	0.90	4.8	0.14
F	**39.6**	**1.13**	26.8	0.77	**3.7**	0.10
G	46.5	1.33	**35.2**	1.01	7.3	0.21
H	**51.2**	**1.47**	34.0	0.97	4.7	0.13
I	43.7	1.25	28.8	0.82	7.0	0.20
J	46.1	1.32	29.7	0.85	4.7	0.13

Explanations: NDF—neutral detergent fibre, ADF—acid detergent fibre, ADL—acid detergent lignin; minimum and maximum values are shown in bold to support comparison.

The data in Table 5 (CP, CL, and CF) confirm that fibre structure, rather than CF alone, is a better descriptor of process kinetics. Batches with high CF and simultaneously low ADL, such as C (CF 24.9% DM, ADL 4.7% DM) and E (CF 23.0% DM, ADL 4.8% DM), remain readily degradable. This is directly reflected in BMP/VS as C 385.7 and E 401.5 m^3 CH_4/Mg VS. Conversely, ADL $\geq$ 7% DM (B, D, G, and I) implies a need for longer HRT, a gentler OLR ramp-up, and, under operational conditions, benefits from blending these batches with material of lower ADL (e.g., C, E, H, and J) to harmonise kinetics. This is consistent with Table 2. Batches D, G, H and J also showed higher EC of at least 9 mS/cm. In combination with more recalcitrant fibre, this increases the risk of osmotic stress in syntrophic communities during sudden feeding increases. Hence, gradual dosing and maintaining alkalinity at 3–5 g $CaCO_3$/L are recommended [50,51].

The information in Table 3 (DM, VS and ash) indicates that the FM-based differences in Table 4 arise from (i) water content (DM), (ii) the amount of biodegradable organic matter (VS/DM), and (iii) fibre recalcitrance (ADL in Table 6). Samples B, D and H, combining elevated DM (33–35%) with moderate ADL (H) or slightly elevated ADL (D), achieved leading FM-based BMP values (114–120 m^3 CH_4/Mg FM). In contrast, C and E offset lower DM through high VS quality and a favourable fibre structure, as shown by BMP/VS. Samples with higher ash (A, F, Table 3) showed a slightly lower calorific value per unit of FM, with average ADF and ADL values. This helps explain why their BMP/VS (A 351.8, F 344.8 m^3 CH_4/Mg VS) ranked below the best-performing batches [52].

From a process perspective, three practical implications follow from Table 6. First, ADL > 7% DM should be treated as a signal to increase HRT and apply a gentler OLR ramp. In mixtures, it is beneficial to target a share of batches with ADL $\leq$ 5% DM (C, E, H, and J) to improve hydrolysis and stability [49]. Second, at NDF $\geq$ 48–50% DM (A, D, and H), particularly when EC is high (Table 2), pre-blending with digestate recirculate is advisable. Where economically justified, cellulolytic and hemicellulolytic enzymes can also be applied during substrate storage [53]. Third, for batches with low ADL and high BMP/VS (C and E), higher short-term OLR may be acceptable, or these batches can be used to support the kinetics of more difficult material (G and D), smoothing methane production [54]. Detergent fibre in Table 6 is therefore central to interpreting process kinetics. NDF defines the load to be treated. ADF reflects the share of the more slowly degradable fraction,

cellulose and lignin. ADL represents a barrier at the operational timescale. This barrier can be mitigated by longer HRT and appropriate size reduction. Based on pH and EC (Table 2), DM, VS and ash (Table 3), BMP on an FM, DM and VS basis (Table 4), and CP, CL and CF fractions (Table 5), the analysed material appears predictable and technically safe. The yields reported earlier align with expectations. Any risks relate mainly to higher lignin and higher salinity in several batches. Both can be managed through appropriate blending, OLR control, and maintaining alkaline buffering capacity [55].

Detergent fibre fractions explain BMP differences across batches, mainly via ADL effects on hydrolysis rate. Low-ADL batches support kinetics, while high-ADL batches require longer HRT and a gentler OLR ramp. Blending can manage fibre recalcitrance and salinity effects without compromising stability.

3.5. Derived Fractions (Hemicellulose, Cellulose, Residual OM) and Estimation of C/N

The results presented in Tables 2–6 indicate that AD performance depends on organic matter composition and nutrient availability, not only on total organic matter content. This subsection presents derived fractions from the detergent fibre system and an approximate C/N ratio. The aim is to link carbohydrate composition and nitrogen availability to BMP variability and operational implications (see Table 7).

Table 7. Composition of the analysed maize silage samples expressed as derived fractions.

Sample	Hemicellulose % DM	Uncertainty (+/−)	Cellulose % DM	Uncertainty (+/−)	Residual OM % DM	Uncertainty (+/−)
A	**22.2**	0.66	**20.6**	0.55	**27.4**	1.24
B	15.6	0.46	24.0	0.64	36.8	1.66
C	16.1	0.48	24.3	0.65	36.5	1.65
D	17.6	0.52	24.4	0.65	31.2	1.41
E	**10.9**	0.32	26.6	0.71	40.1	1.81
F	12.8	0.38	23.1	0.61	38.5	1.74
G	11.3	0.33	27.9	0.74	35.7	1.61
H	17.2	0.51	**29.3**	0.78	29.5	1.33
I	14.9	0.44	21.8	0.58	**40.8**	1.84
J	16.4	0.48	25.0	0.66	36.2	1.63

Explanation: minimum and maximum values are shown in bold to support comparison.

Table 7 breaks the material into carbohydrate-derived and soluble fractions. Hemicellulose ranged from 10.9 to 22.2% DM, cellulose from 20.6 to 29.3% DM, and residual organic matter (residual OM) from 27.4 to 40.8% DM. The corresponding uncertainties were approximately ±0.3–0.7, ±0.6–0.8, and ±1.2–1.8 percentage points, respectively.

As hemicelluloses hydrolyse faster than cellulose, and residual OM largely comprises readily fermentable compounds, these fractions explain early fermentation behaviour and early biogas formation, as well as BMP/VS in Table 4 [56]. Batches with high residual OM (E 40.1%, I 40.8%, F 38.5%, J 36.2%, and B 36.8%) are typically easier to degrade at the start. They supply rapidly available substrate, which can shorten lag and support stable methanogenesis (cf. Table 2). This is consistent with the high BMP/VS of E and the solid results for B, F and J in Table 4. It should be noted that a readily degradable fraction can increase the rate of VFA formation. In practice, these batches should be fed with digestate recirculation and a gradual increase in OLR, especially when EC is elevated, as in J (10.3 mS/cm) [57].

Samples with high cellulose (H 29.3%, G 27.9%, E 26.6%, J 25.0%, and C 24.3%) may show slower early kinetics because cellulose requires efficient consortial hydrolysis. This does not necessarily reduce the final potential. Sample G illustrates this pattern, as it achieved high BMP/VS despite high ADF and ADL (Table 6). This suggests that, with sufficiently long HRT and an active inoculum, cellulose mainly affects the rate rather than the ultimate yield. Similarly, H combines high cellulose (29.3% DM) with low lignin (ADL 4.7% DM) [58,59]. This supports a strong fresh-mass outcome in Table 4 and aligns with high DM in Table 3 and a favourable hemicellulose share in Table 7.

Hemicellulose is a key kinetic component. Higher hemicellulose (A 22.2%, H 17.2%, D 17.6%, and J 16.4%) can support a smoother transition to methanogenesis if ADL is not excessive. For this reason, Table 7 should be interpreted together with Table 6. High hemicellulose with low ADL indicates more favourable hydrolysis and often higher BMP/VS. Even moderate hemicellulose with ADL at or above 7% DM suggests a need for longer HRT or hydrolysis support. Alongside Table 5, the data indicate that Weende CF alone is not decisive. Cell-wall structure is the key factor. In C and E, high CF coincides with low lignin and high residual OM, which explains their fermentation performance [60].

When interpreted alongside Tables 2 and 3, these fractions clarify fresh-mass expectations and operational handling. Higher DM combined with substantial residual OM supports higher methane yield per tonne of fresh material. Higher ash reduces fuel value per unit mass and requires tighter OLR control. High EC combined with higher cellulose supports blending and gentler introduction. Where cellulose is at or above 27–29% DM and or ADL is at or above 7% DM, HRT should be longer, and OLR ramp-up should be more cautious. Where residual OM is at or above 38–41% DM, rapid potential can be utilised, but feeding should include recirculation and FOS and TAC control. Where EC is higher, blending with lower-EC and lower-ADL material helps balance osmotic load and hydrolysis. Table 7 explains why E, C and G lead in BMP/VS, why H and D perform strongly on a fresh-mass basis due to higher DM, and why risks reflect combined salinity and lignin effects [61].

Elemental values in Table 8 complement the assessment of the analysed maize silages by linking substrate chemistry to the previously observed methane yield and kinetics. Nitrogen ranged from 1.0 to 1.8% DM, while carbon ranged from 42.9 to 45.6% DM. The variability in carbon was small (about $\pm$2.7 percentage points). This suggests that carbon form and C/N matter more than total carbon content. The approximate molar C/N ranged from 24.1 (A) to 41.3 (D and E), with intermediate values for most samples (30–39).

In operational terms, two practical ranges emerge. Lower C/N (A 24.1, F 29.9, H 30.7, C 30.1, and J 32.1) supports microbial growth and may shorten lag. When combined with higher CP in Table 5, especially in A, TAN and OLR control is needed to avoid ammonia-related effects. Conversely, samples with higher C/N (D 41.3, E 41.3, I 39.2, and B 38.5) are less prone to ammonia inhibition, but may become nitrogen-limited if dosed at a high share without co-digestion with N-richer substrates [62]. Comparison with earlier tables shows a consistent pattern. D and E performed strongly on a fresh-mass basis despite high C/N, due to higher DM in D and high residual OM with moderate lignin in E. A combines low C/N with high CP and elevated ash, which aligns with its moderate BMP/VS and higher control needs as OLR increases. C and H show stable profiles. In C, low lignin and a substantial share of hydrolysable fractions support high BMP/VS despite lower DM. In H, higher DM and low lignin support an above-average BMP on a fresh-mass basis [63]. Elevated EC can coincide with slower hydrolysis, especially when ADL is higher. Blending with lower-ADL batches and a gentle OLR ramp-up is recommended. A practical approach is to blend higher C/N batches with lower C/N batches to keep the mixture near 25–30, up to 33. At lower C/N, avoid sudden OLR increases and monitor TAN and FAN.

At higher C/N, ensure a minimum nitrogen supply. In all cases, carbon form should be considered [64]. Where ADL is at or above 7% DM or cellulose is at or above 27–29% DM (Tables 6 and 7), kinetics may constrain short-term production, so HRT should be increased and or hydrolysis support applied.

Table 8. Elemental composition of the analysed maize silage samples.

Sample	Nitrogen % DM	Uncertainty (+/−)	Carbon % DM	Uncertainty (+/−)	C/N (Molar, Approx.)	Uncertainty (+/−)
A	**1.8**	0.04	**42.9**	1.09	**24.1**	0.64
B	1.2	0.03	45.1	1.15	38.5	1.03
C	1.5	0.04	45.1	1.15	30.1	0.80
D	1.1	0.02	44.2	1.13	41.2	1.10
E	**1.0**	0.02	43.2	1.10	**41.3**	1.10
F	1.4	0.03	43.1	1.10	29.9	0.80
G	1.2	0.03	44.2	1.13	35.9	0.96
H	1.4	0.03	43.3	1.10	30.7	0.82
I	1.2	0.03	**45.6**	1.16	39.2	1.04
J	1.4	0.03	44.2	1.13	32.1	0.86

Explanation: minimum and maximum values are shown in bold to support comparison.

Overall, Table 8 confirms that the analysed silages fall within a favourable C/N range for AD. In conjunction with Tables 2–7, these data support a blend design that stabilises kinetics and maintains high methane yield [65,66].

The derived fractions indicate that early kinetics are shaped by residual OM and hemicellulose, while cellulose and lignin constrain the rate. C/N informs nitrogen availability and TAN risk, but carbon form remains decisive for hydrolysis. Stable performance is expected when blends balance salinity, lignin and nutrient supply.

3.6. Macro- and Microelement Profiles of Maize Silages—Nutritional and Inhibitory Context of the Process

The elemental profile reported in Tables 9–12 refines the quality assessment of the analysed maize silages and supports the interpretation of the methane fermentation performance and kinetics observed earlier (Table 4). This interpretation is made in relation to physicochemical properties (pH and electrical conductivity (EC)—Table 2), the dry matter/organic matter/ash balance (DM/OM/ash—Table 3), the CP–CL–CF macrofraction composition (Table 5), the detergent and derived fractions (neutral detergent fibre, acid detergent fibre, acid detergent lignin, hemicellulose, cellulose, and residual organic matter—Tables 6 and 7), and the carbon-to-nitrogen ratio (C/N—Table 8).

In general, macroelements (Ca, P, K, Mg, Na, S and Cl) determine the buffering capacity and osmotic pressure of the feed, whereas micro- and ultra-trace elements (Fe, Mn, Zn, Cu, Ni, Mo, Co and Se) modulate the activity of key enzymes within the methanogenic consortium [67]. Their levels in the present samples fall within ranges typical for maize silage, yet differences between batches are relevant from a process perspective. In operational terms, these differences affect process stability, expressed as the capacity to increase the organic loading rate safely without inducing osmotic stress, without episodes of volatile fatty acid accumulation, while maintaining stable biogas quality.

Table 9. Major macronutrients related to mineral balance and buffering (Ca, P, K, and Mg) in maize silage (g/kg DM).

Sample	Ca (g/kg DM)	Unc. (+/−)	P (g/kg DM)	Unc. (+/−)	K (g/kg DM)	Unc. (+/−)	Mg (g/kg DM)	Unc. (+/−)
A	3.4	0.13	2.2	0.82	12.2	0.45	1.5	0.05
B	2.4	0.09	2.4	0.87	**13.3**	0.49	**1.3**	0.05
C	2.4	0.09	2.3	0.85	11.4	0.42	1.4	0.05
D	3.3	0.13	2.1	0.79	12.3	0.45	**1.9**	0.07
E	2.4	0.09	1.8	0.66	12.9	0.47	1.5	0.05
F	2.7	0.10	2.1	0.78	11.5	0.42	1.4	0.05
G	**3.5**	0.13	**1.7**	0.65	12.2	0.45	1.5	0.06
H	**1.8**	0.07	2.4	0.90	11.3	0.42	1.6	0.06
I	2.7	0.10	2.0	0.73	**9.4**	0.35	1.7	0.06
J	3.4	0.12	**2.5**	0.89	11.8	0.43	1.5	0.06

Explanations: Unc.—uncertainty, DM—dry matter; minimum and maximum values are shown in bold to support comparison.

Table 10. Salinity- and sulphur-related macronutrients (Na, S, and Cl) in maize silage (g/kg DM).

Sample	Na (g/kg DM)	Unc. (+/−)	S (g/kg DM)	Unc. (+/−)	Cl (g/kg DM)	Unc. (+/−)
A	0.53	0.020	1.5	0.06	3.2	0.12
B	**0.21**	0.008	1.7	0.06	4.0	0.15
C	0.33	0.012	1.4	0.05	3.1	0.11
D	0.39	0.014	1.5	0.05	3.5	0.13
E	0.39	0.014	1.5	0.06	3.6	0.13
F	0.63	0.023	1.6	0.06	**3.0**	0.11
G	0.45	0.017	**1.3**	0.05	3.5	0.13
H	0.65	0.024	1.8	0.07	**4.5**	0.16
I	0.39	0.014	1.5	0.05	3.5	0.13
J	**0.66**	0.024	**1.9**	0.07	3.8	0.14

Explanations: Unc.—uncertainty, DM—dry matter; minimum and maximum values are shown in bold to support comparison.

Within the dominant cation and anion group (see Tables 9 and 10), potassium content is high, yet still typical for maize (K ≈ 9.4–13.3 g/kg DM). Calcium and magnesium are present at moderate levels (Ca ≈ 1.8–3.5 g/kg DM, Mg ≈ 1.4–1.9 g/kg DM), with phosphorus at ≈1.8–2.4 g/kg DM. This composition supports buffering capacity once the feed is blended with digestate recirculate, and the pH values of 3.8–4.2 reported in Table 2 do not represent a risk after dilution. At the same time, batches with higher conductivity (EC ≥ 9 mS/cm, D, G, H and J in Table 2) show an increased Na/Cl/S ionic load (Table 10, Na up to 0.66 g/kg DM, Cl up to 4.5 g/kg DM, and S up to 1.9 g/kg DM), which explains the higher EC observed for these materials. From an operational perspective, this signals the need for a gentler OLR ramp-up and blending with lower-EC batches (e.g., B and C), particularly when lignin share (ADL) is also elevated (G and D—Table 6). The combined effect of higher salinity and a more recalcitrant fibre structure commonly slows hydrolysis [68]. This can slow the build-up of biogas production, without necessarily reducing BMP/VS (sample G in Tables 4, 6 and 7). It should also be noted that total sulphur

(S, 1.3–1.9 g/kg DM) indicates an increased risk of H_2S formation in biogas. For these batches, early use of an iron-based sorbent or dosing Fe(II) or Fe(III) in the liquid phase is justified [69].

Table 11. Trace metals relevant to process stability and sulphide control (Fe, Mn, Zn, and Cu) in maize silage (mg/kg DM).

Sample	Fe (mg/kg DM)	Unc. (+/−)	Mn (mg/kg DM)	Unc. (+/−)	Zn (mg/kg DM)	Unc. (+/−)	Cu (mg/kg DM)	Unc. (+/−)
A	176.7	6.51	106.1	3.91	26.8	0.99	11.2	0.41
B	156.6	5.77	66.5	2.45	41.8	1.54	**3.6**	0.13
C	207.0	7.63	105.5	3.89	21.9	0.81	4.6	0.17
D	203.4	7.50	48.8	1.80	**51.9**	1.91	7.0	0.26
E	128.2	4.73	110.7	4.08	51.5	1.90	8.1	0.30
F	226.3	8.34	75.4	2.78	39.3	1.45	6.7	0.25
G	246.5	9.09	85.4	3.15	46.1	1.70	**13.5**	0.50
H	**91.5**	3.37	**112.6**	4.15	46.2	1.70	6.1	0.22
I	**258.2**	9.52	**36.7**	1.35	42.2	1.56	4.8	0.18
J	243.3	8.97	96.3	3.55	**19.8**	0.73	11.5	0.42

Explanations: Unc.—uncertainty, DM—dry matter; minimum and maximum values are shown in bold to support comparison.

Table 12. Ultra-trace elements supporting methanogenesis (Ni, Mo, Co, and Se) in maize silage (mg/kg DM).

Sample	Ni (mg/kg DM)	Unc. (+/−)	Mo (mg/kg DM)	Unc. (+/−)	Co (mg/kg DM)	Unc. (+/−)	Se (mg/kg DM)	Unc. (+/−)
A	**2.1**	0.08	0.67	0.025	**0.11**	0.004	0.07	0.003
B	1.0	0.04	**1.17**	0.043	0.13	0.005	0.06	0.002
C	0.9	0.03	0.78	0.029	0.13	0.005	0.05	0.002
D	1.2	0.04	0.72	0.027	0.14	0.005	0.07	0.003
E	1.1	0.04	0.81	0.030	0.15	0.006	**0.09**	0.003
F	**0.5**	0.02	0.92	0.034	0.17	0.006	**0.03**	0.001
G	1.0	0.04	0.43	0.016	**0.11**	0.004	0.07	0.003
H	1.0	0.04	0.58	0.021	0.16	0.006	0.04	0.001
I	1.6	0.06	0.89	0.033	**0.18**	0.007	0.08	0.003
J	**2.1**	0.08	**0.57**	0.021	0.14	0.005	0.07	0.003

Explanations: Unc.—uncertainty; DM—dry matter; minimum and maximum values are shown in bold to support comparison.

The role of iron and other microelements (Table 11) is twofold. They serve as nutrients for microbial consortia and act as internal conditioning agents, for example, through sulphide precipitation [69]. Iron ranges from 92 to 258 mg/kg DM, manganese from 37 to 113 mg/kg DM, zinc from 20 to 52 mg/kg DM, and copper from 3.6 to 13.5 mg/kg DM. At these levels, iron availability promotes the binding of hydrogen sulphide as FeS, which stabilises the gas phase and limits sulphide-related inhibition. The elevated Fe observed in batches F, G, I and J may partly offset a higher S and Cl load (H and J). This can facilitate biogas quality control without excessive demand on desulphurisation. Zinc and copper remain within ranges generally regarded as safe. Their accumulation in the digester should

be monitored, yet at the concentrations measured in the substrate, the risk of toxicity is low, particularly where sulphides limit the free-ion fraction [69].

Ultra-trace elements critical for methanogenesis (Table 12), including Ni, Co, Mo and Se, occur at levels consistent with the requirements of the methane pathway enzymes (Ni in cofactor F_{430}, Mo in formate dehydrogenases, Co in methyltransferases, and Se in selenoenzymes) [70]. Although the data refer to contents in the solid phase (mg/kg DM), the operationally relevant parameter is the dissolved concentration in the digester liquor. Nevertheless, relative differences between batches remain informative. Samples with higher Ni (A, J and I, up to 2.1 mg/kg DM) and Co (0.14–0.18 mg/kg DM in D, E, F, H and I) tend to support a shorter methanogenic lag phase and improved resilience to loading fluctuations. This is consistent with the strong fermentation class of E and the high fresh-matter productivity of D and H, where the effect of higher DM also contributes (Table 3). Molybdenum shows greater variability (0.43–1.17 mg/kg DM). Higher values (B and F) support formate-related pathways, which may explain stable fermentation despite differences in fibre properties (B with higher ADF and F with lower ADL) [71]. Selenium remains at trace levels (0.03–0.09 mg/kg DM). Within this range, it is supportive and rarely limiting. The Ni, Co, Mo and Se pattern indicates no clear nutritional gaps, and minor deficits can be mitigated by blending batches.

When the mineral profile is considered alongside the earlier tables, a coherent process picture emerges. Batches with higher EC (Table 2, D, G, H and J) generally also show higher Na/Cl/S (Table 10). They require a gentler OLR increase and pre-blending with digestate recirculate, particularly where cellulose and ADL are elevated (Tables 6 and 7, G and, to a lesser extent, D). Substrates with high residual OM and a favourable fibre structure (E and C, Table 7) combine a supply of readily available carbon with moderate salinity. This explains their high BMP/VS (Table 4) and favourable start-up kinetics, supported by adequate microelement availability [72]. In contrast, silages with low C/N (A, F and H, Table 8), combined with increased Na/Cl (F and H) and high CP (A), may promote faster formation of VFAs and total ammoniacal nitrogen. In practice, these batches benefit from alkaline buffering and a moderate substrate-to-inoculum ratio. The presence of Fe (Table 11) and Mo/Co/Ni (Table 12) supports methanogenic activity under transient loading variations.

From an operational viewpoint, three pragmatic recommendations follow. First, salinity management: batches H and J (higher Na/Cl/S and the highest EC), as well as D and G (high EC with a more recalcitrant fibre structure), should be introduced gradually, blended with B/C/E, and operated at an alkalinity of 3–5 g $CaCO_3$/L. In parallel, the intrinsic Fe load can be used to reduce H_2S formation [73]. Second, microelement balancing: where the mixture is dominated by batches with lower Ni/Co (e.g., B, C, G and H), it is beneficial to add a fraction of feedstock richer in these elements (A, I and J) or, where plant practice allows, to apply moderate supplementation of Ni/Co salts in the liquid phase [74]. Third, coupling with carbon form: where hemicellulose and residual OM are high (E, I, F and J), the potential for rapid fermentation can be utilised, but FOS/TAC should be controlled. Where cellulose and/or ADL are elevated (H, G and partly D), longer hydraulic retention time (HRT) and/or enzymatic support is advantageous. Within these boundaries, the mineral profile in Tables 9–12 does not constrain the process. Instead, it helps to explain why the analysed silages deliver stable and predictable yields reported in Table 4. Differences between batches are driven mainly by the interaction of salinity, buffering and fibre recalcitrance, while microelement availability remains sufficient to sustain full enzymatic activity of methanogenic pathways [75].

The mineral profile in Tables 9–12 supports stable AD operation and helps interpret yield differences in Table 4. High EC batches align with higher Na, Cl and S and require gentler OLR ramp-up and blending, especially when fibre recalcitrance is higher. Trace and

ultra-trace elements appear sufficient across the dataset, while Fe can support sulphide control and process resilience.

3.7. Biogas Composition and OM/VS Conversion

Following the evaluation of the mineral background (Tables 9–12), the next step is to assess the process outcome in the BMP test. This background affects osmotic pressure, buffering capacity, and the availability of trace elements for methanogenesis. For this purpose, biogas composition and the extent of organic matter degradation expressed as OM/VS conversion were analysed (see Table 13). This approach complements the BMP results (Table 4) by separating gas quality from the depth of substrate degradation.

Table 13. Methane content in biogas and OM/VS conversion for the analysed maize silage samples.

Sample	CH_4 Content (% *v*/*v*)	Uncertainty (+/−)	Conversion (%)	Uncertainty (+/−)
A	54.2	1.60	75.5	2.91
B	**56.8**	1.68	78.1	3.01
C	54.1	1.60	**85.8**	3.30
D	56.5	1.67	75.5	2.91
E	55.4	1.64	83.7	3.22
F	54.2	1.60	**74.6**	2.87
G	55.2	1.63	82.4	3.17
H	55.8	1.65	77.2	2.97
I	54.2	1.60	82.9	3.19
J	**52.1**	1.54	78.3	3.02

Explanation: minimum and maximum values are shown in bold to support comparison.

The results in Table 13 summarise both biogas quality (CH_4 share) and the degree of organic matter degradation (conversion). Methane content ranged from 52.1 to 56.8% *v*/*v* (mean ≈ 55%), which is typical for maize silage [1,8,30]. The uncertainty of a single determination was approximately ±1.6 percentage points. The highest CH_4 fractions were recorded for B (56.8%), D (56.5%) and H (55.8%). This aligns with their compositional profile. These batches showed relatively higher dry matter (DM, Table 3) and a favourable energy contribution of fractions, including crude lipids (CL) in D and B (Table 5). This can increase the methane fraction in the gas. In D, this effect occurs despite elevated acid detergent lignin (ADL, Table 6), which slows hydrolysis but does not necessarily reduce the final CH_4 fraction. The lowest CH_4 fraction was observed for J (52.1%). This batch also had the highest electrical conductivity (EC, Table 2), which indicates a higher $Na^+/Cl^-/S$ load (Table 10). Such a profile can increase the relative CO_2 contribution in the early phase and can coincide with less favourable fibre properties (Tables 6 and 7). This explains the lower CH_4 share despite adequate DM [76,77].

The second dimension of Table 13, conversion (75–86%, uncertainty ± 3.0 percentage points), reflects the form of carbon and the cell-wall fraction composition described earlier. The conversion leaders, C (85.8%), E (83.7%), I (82.9%), and G (82.4%), match the batches with high BMP/VS in Table 4. In Tables 6 and 7, they combine low or moderate ADL with a substantial share of hydrolysable cellulose and hemicellulose, as well as a notable residual organic matter fraction, particularly in E and I. Lower lignin barrier and a higher share of readily fermentable compounds support higher BMP and result in higher conversion [78]. By contrast, A (75.5%) and F (74.6%) show the lowest conversion. They also have elevated ash content (Table 3) and only average fraction quality (Tables 5–7). Their mineral fraction

dilutes the biodegradable load, which reduces the degree of degradation. Batch D (75.5%) combines a high CH_4 fraction with reduced conversion. This pattern is consistent with its higher energy fraction profile, including CL, and an ADL level of 7.4% DM (Table 6). The limitation relates to the hydrolysis rate and depth, not to gas quality [79].

Inclusion of the elemental profile (Tables 9–12) and the C/N balance (Table 8) clarifies the main operational risks and indicates control options. Batches with higher C/N (D, E, I, and B) are less prone to ammonia-related stress. With an appropriate substrate-to-inoculum ratio (ISR), they support the selection of a hydraulic retention time (HRT) that enables complete hydrolysis, which is reflected in the high conversion of E and I. Batches with lower C/N (A, F, H, and C) can show rapid initial activity but require control of total ammoniacal nitrogen (TAN), free ammonia nitrogen (FAN), and FOS/TAC to avoid acidic peaks that could lower conversion, as observed for A and F. High EC (D, G, H, and J, Table 2) corresponds to increased Na/Cl/S (Table 10) and can delay attainment of full conversion [80]. This effect is stronger when ADL is ≥~7% DM (D and G). In such cases, blending with low-ADL batches (C, E, and H) and extending HRT can restore conversion above 80%. A further stabilising factor is the availability of Ni/Co/Mo/Se (Table 12). No clear nutritional gaps are evident in the dataset. Batches richer in Ni/Co (A, I, J) can support mixtures containing more recalcitrant fibre.

These patterns can be translated into operational rules. If a higher CH_4 fraction is the priority, mixtures with higher DM and moderately higher CL are preferred, while avoiding excessive long-chain fatty acids and maintaining buffering capacity [81]. This profile is represented by B, D, and H. If high conversion is the priority, low ADL and higher residual OM should be prioritised [82]. Longer HRT and reduced salinity are beneficial, as shown by C, E, and I. Batches with high EC and/or high ADL (D, G, and J) should be introduced gradually, blended with C/E/H, and operated at an alkalinity of 3–5 g $CaCO_3$/L. The differences in Table 13 exceed their uncertainties, typically by 3–5 percentage points between extremes. They are therefore technologically relevant [83]. Within this variability, the analysed silages remain predictable and controllable. The CH_4 fractions and conversion levels are consistent with the logic of Tables 2–12.

Taken together, biogas composition and conversion separate gas quality from degradation depth. Higher CH_4 share aligns with higher DM and CL, while higher conversion aligns with low ADL and higher residual OM. High EC and higher ADL can delay conversion, so blending and longer HRT support stable outcomes.

3.8. Kinetic Modelling of BMP Curves: Gompertz and First-Order Models

To quantify differences among samples A–J, not only in terms of the final BMP, but also in terms of the rate of CH_4 accumulation and the time required to reach near-complete conversion over 0–50 days, methane cumulative curves were described using two complementary empirical models. These were the modified Gompertz model and the first-order Cone model with m = 1 (Equations (1) and (2), see Materials and Methods Section 2) [7,24]. The present subsection, therefore, focuses on the interpretation of the fitted curves and their technological relevance in relation to the BMP profiles (see Figures 2 and 3). To address the observed differences in curve onset and shape in Figures 2 and 3 and to enable a quantitative comparison across batches, the fitted kinetic parameter values from both models are reported explicitly in Table 14.

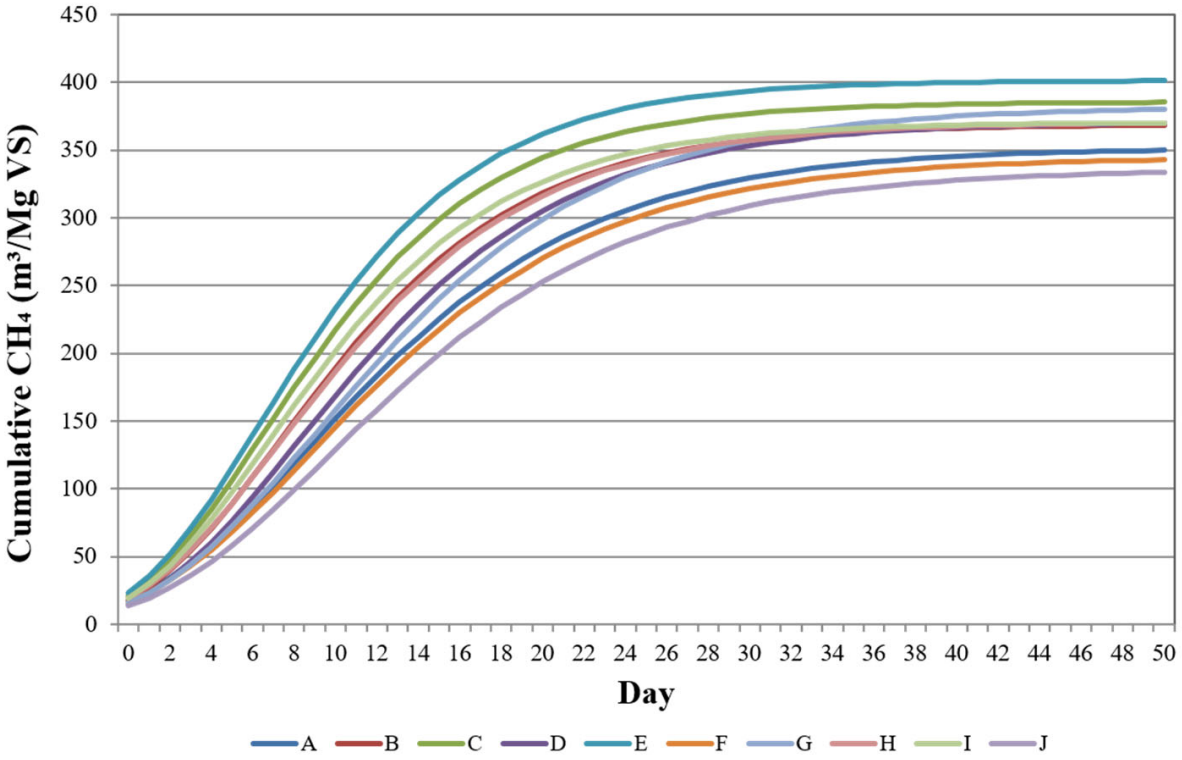

Figure 2. Cumulative methane production curves for samples A–J over 0–50 days fitted with the modified Gompertz model.

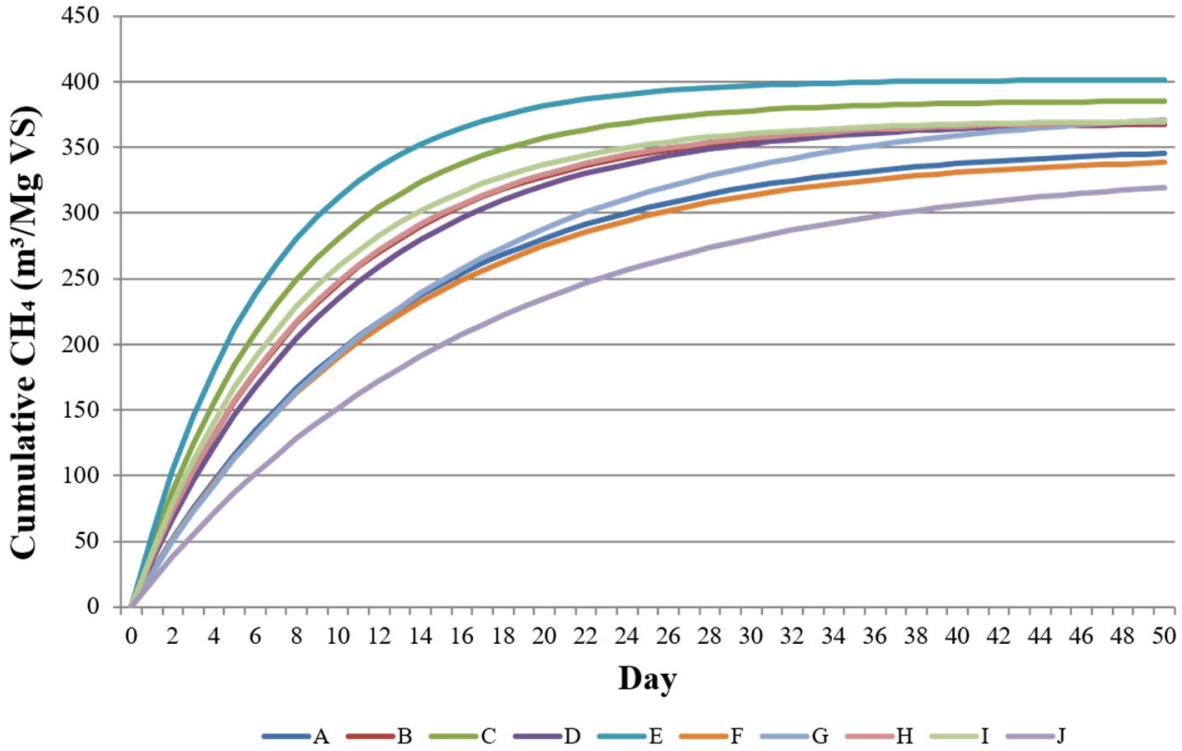

Figure 3. First-order Cone modelling (m = 1) of cumulative methane production for samples A–J (0–50 days).

Table 14. Key fitted kinetic parameters of the modified Gompertz and first-order Cone (m = 1) models for maize silage batches (A–J).

Sample	G_{max}	R_{max}	λ	B_0 (Gomp)	t_{50} (Gomp)	t_{90} (Gomp)	B_0 (First-Order)	k	t_{50} (First-Order)	t_{90} (First-Order)
A	351.8	16.5	0.8	17.338	12.084	26.724	351.8	0.08	8.664	28.782
B	369.0	20.5	0.7	17.983	10.225	22.588	369.0	0.11	6.301	20.933
C	385.7	23.0	0.4	21.215	9.333	20.830	385.7	0.13	5.332	17.712
D	371.1	19.0	1.1	15.619	11.365	24.791	371.1	0.10	6.931	23.026
E	401.5	24.5	0.3	23.063	9.046	20.286	401.5	0.15	4.621	15.351
F	344.8	16.0	0.9	16.410	12.289	27.079	344.8	0.08	8.664	28.782
G	382.3	18.0	1.2	16.066	12.361	26.952	382.3	0.07	9.902	32.894
H	370.6	21.5	0.5	19.567	9.661	21.491	370.7	0.12	5.776	19.188
I	370.7	20.0	0.6	19.050	10.436	23.150	370.6	0.11	6.301	20.933
J	336.2	15.0	1.4	13.415	13.149	28.568	336.2	0.06	11.552	38.376

Explanations:

- Units: G_{max} and B_0 (m^3 CH_4/Mg VS), R_{max} (m^3 CH_4/Mg VS·d), λ (d), k (d^{-1}), t_{50} and t_{90} (d),
- G_{max}: asymptotic methane potential from the modified Gompertz model,
- R_{max}: maximum methane production rate from the modified Gompertz model,
- λ: lag phase duration from the modified Gompertz model,
- B_0 (Gompertz): fitted offset parameter in the modified Gompertz formulation,
- t_{50} (Gompertz) and t_{90} (Gompertz): times to reach 50% and 90% of G_{max} derived from the fitted Gompertz curve,
- B_0 (first-order): asymptotic methane potential from the first-order Cone model (m = 1),
- k: first-order rate constant from the first-order Cone model (m = 1),
- t_{50} (first-order) and t_{90} (first-order): calculated from k as ln(2)/k and ln(10)/k, respectively,
- Fit quality: report one concise metric for each model (e.g., R^2 for Gompertz and Cone, or RMSE for Gompertz and Cone),

Table 14 summarises the fitted kinetic descriptors for all batches. The modified Gompertz model separates start-up behaviour (λ), maximum production rate (R_{max}) and asymptotic methane potential (G_{max}), while the first-order Cone model provides a parsimonious description using B_0 and k. The derived times t_{50} and t_{90} support benchmarking and HRT-oriented planning. The asymptotes G_{max} and B_0 are consistent with the VS-based BMP yields, which supports the validity of the fits and indicates no systematic overestimation of methane potential.

The Gompertz-based description of the BMP profiles is shown in Figure 2. The model separates start-up delay (λ), the main production phase (R_{max}), and the asymptotic BMP/VS (G_{max}). These parameters can be linked to measurable feedstock properties (EC/salinity, ADL, the proportion of soluble fractions, and the supply of trace elements Ni/Co/Mo/Se) [84]. The empirical data are fully consistent with this mechanistic interpretation.

Depending on the sample, the asymptotic values G_{max} fall within approximately 333–401 m^3 CH_4/Mg VS, reflecting the previously determined BMP/VS and the differences in organic matter quality (SMO, ash, and ADL). Already within days 1–2, G(t) increases markedly, which indicates a short lag and good soluble substrate availability. In practice, λ is on the order of 0–2 days. Longer delays are not observed, even though several batches

show elevated electrical conductivity (EC), which typically extends the lag phase. The steepest part of the curves, corresponding to the vicinity of R_{max}, occurs between days 8 and 16. Thereafter, the accumulation rate decreases, and the trajectories smoothly transition into a hydrolytic tail [85].

The half-conversion horizon (t_{50}, when $G(t) = 0.5\ G_{max}$) further confirms only modest kinetic differences among batches [4]. For most samples, t_{50} is around days 10–13. Samples richer in soluble fractions tend to reach t_{50} earlier and show higher R_{max}. Batches with higher ADL and or higher EC show a longer tail and a later t50 at comparable G_{max}. This reflects the typical pattern of rapid start-up combined with slower completion of anaerobic conversion, in which the Gompertz model performs better than simple mono-exponential models because it captures both osmotic and adaptation-related delay and the asymmetry associated with cell-wall hydrolysis [5].

In operational terms, the Gompertz parameters provide useful decision-support indicators. The short λ suggests that the tested silages do not require special conditioning beyond standard blending with recirculated digestate. Higher R_{max} in batches richer in soluble fractions supports a more cautious OLR ramp-up primarily during the first week in order to avoid short-term peaks in VFAs [86]. Furthermore, G_{max} values towards the end of days 41–50 indicate that HRT windows of approximately 40–50 days ensure near-complete realisation of BMP potential. For batches with higher ADL or EC, longer retention or hydrolysis support may be justified. This can be achieved by enzymatic treatment or pre-mixing. Overall, the Gompertz fits confirm the favourable fermentability of maize silage and allow feedstock properties (EC, ADL, and the share of soluble fractions) to be translated quantitatively into start-up behaviour, safe loading strategies, and the required HRT, which is central to informed digester operation [87].

In this study, the methane cumulative curves for samples A–J (0–50 days) obtained in the batch BMP test were also described using the first-order Cone model with m = 1, in accordance with Equation (2), where the fitted parameters are the asymptote (B0) and the rate constant (k). The corresponding first-order fits are shown in Figure 3.

The model does not include an explicit lag parameter (λ). Any short start-up delay is effectively absorbed into k. Lower k corresponds to a slower start-up and a longer tail. The model is parsimonious and generalises the kinetics of relatively homogeneous substrates under predominantly hydrolytic control. Importantly, in practical terms, it enables the time to half conversion and the time required to reach a high degree of conversion, such as 90%, to be linked directly to the rate parameter. Here, t_{50} was calculated from the fitted k values using Equation (3) (Section Materials and Methods) and used to interpret the half-conversion horizon.

The empirical behaviour is typical of first-order kinetics. From day 0, G(t) increases monotonically and smoothly without a distinct induction phase, reaching approximately 50% of the asymptote around days 10–12. This implies k values in the mesophilic range and reproduces the steep segment over days 1–15 and the tail after day 30. The B_0 asymptotes derived from the 50-day trajectories are consistent with the expected BMP/VS for maize silage and differ among samples in a process-relevant manner. This pattern supports three energetic classes based on B_0. These are high potential, medium potential, and lower potential. At the same time, the trajectories are mono-exponential, without an early plateau or an inflexion indicative of two-stage behaviour. This is the condition under which the Cone model (m = 1) reproduces the data faithfully.

From the standpoint of technological interpretation, B_0 provides a reliable indicator of the energetic class of a given batch on a VS basis and translates directly into the outcome on a fresh-matter basis once DM and SMO are taken into account. The parameter k reflects both the start-up and the hydrolysis-limited completion phase. Mesophilic-range values

of 0.058–0.069 d^{-1} suggest that the minimum HRT required to reach at least 90% of B_0 should exceed approximately 30–40 days. This aligns with curve stabilisation after around day 40. For batches with lower B_0 and or a slower approach (A, F, and J), a slight extension of HRT or support for hydrolysis may be beneficial. For high-B_0 batches (E and C), shorter operational windows can be planned without yield loss.

The limitations of this model follow from its simplicity. The lack of an explicit λ parameter prevents the separate quantification of adaptation and osmotic delay and effective rate. A single k does not distinguish rapidly biodegradable fractions from slow fractions. In practice, if other feedstock batches exhibited a pronounced lag or a clear change in rate, the Cone model (m = 1) would be too rigid. Such a problem is not apparent in the present dataset. The curves are kinetically homogeneous, and the first-order model therefore describes the data well.

In summary, the first-order Cone model (m = 1) supports rapid benchmarking via B_0, k, t_{50} and t_{90}. Under conditions without a distinct induction phase and with mono-exponential trajectories, its fit is adequate for design and operational purposes. For scenarios with a pronounced lag and or differentiated fast and slow fractions, the modified Gompertz model or a two-fraction first-order model remains the recommended generalisation, as these approaches separate start-up effects from fibre-structure constraints [86].

Both models support operational interpretation of BMP curves. Gompertz highlights start-up delay and peak rate, while Cone links conversion times directly to k. The dataset shows short lag, modest between-batch kinetic differences, and a hydrolytic tail that guides HRT planning. In practice, Cone is suitable for rapid benchmarking and HRT setting, whereas Gompertz is more informative when start-up dynamics and adaptation effects must be managed.

4. Discussion

The results presented in this article show that the anaerobic digestion kinetics of maize silage are governed by two concurrent mechanisms. Gas production starts rapidly due to the presence of soluble fractions, including sugars, volatile acids, and part of the starch, oligosaccharides, and hemicellulose. This initial phase is followed by a slower, structurally limited hydrolysis of the plant cell wall, where cellulose is protected by lignin. This dual nature of the substrate explains why two complementary empirical models, the modified Gompertz model and the first-order model (Cone, m = 1), describe the BMP curves in this dataset most effectively [9]. The BMP/VS results also indicate that structural constraints, particularly lignin, affect conversion rate more strongly than the final potential. Samples with an elevated lignin fraction can still reach high BMP/VS provided that incubation or retention time is sufficient and the inoculum remains active.

The modified Gompertz model separates three key features of the trajectory: λ (lag time), R_{max} (maximum production rate), and G_{max} (asymptote, i.e., BMP on a VS basis). In the analysed samples, the short lag and the steep rise during days 1–12 are consistent with a high share of readily fermentable material, including residual OM and hemicellulose (Table 7). By contrast, differences in the extent of late-stage tailing reflect hydrolytic resistance associated with ADL and ADF (Table 6). The parameter λ is sensitive to osmotic pressure, reflected by EC (Table 2) and the ionic profile Na/Cl/S (Table 10), as well as to the inoculum condition. R_{max} increases with a higher supply of soluble compounds and with adequate support of methanogenesis by trace elements (Ni, Co, Mo, and Se; Table 12). As a result, the Gompertz model yields parameters that are directly useful in operation, including t_{50} and t_{90}, guidance for OLR ramp-up, and an assessment of sensitivity to salinity [74] (Table 14). It should also be noted that pH and EC need not be closely correlated in this dataset. pH mainly reflects silage maturity and stability through

the acid profile, whereas EC indicates mineral salt load and the associated osmotic risk. These two parameters should therefore be interpreted independently when considering λ and start-up stability.

The first-order Cone model (m = 1) is parsimonious, with only G_∞ and k, and performs well when the trajectory is mono-exponential. This requires the absence of a distinct, prolonged lag phase and no clear change in rate. In the present data, the model reproduces the smooth approach to the asymptote after days 30–40. G_∞ provides a clear measure of energetic quality on a VS basis, consistent with BMP/VS in Table 4, whereas k summarises both the initial process pace and the rate of attenuation of methane production. For clarity, k was obtained as a fitted model parameter, whereas characteristic times were derived subsequently from k. The model, therefore, enables rapid benchmarking of batches. Higher k tends to coincide with higher residual OM and hemicellulose (Table 7) and lower ADL (Table 6). By contrast, salinity indicators (EC and Na/Cl/S) generally decrease k by extending the adaptation period. The characteristic times follow directly from k, with $t_{50} = \ln 2/k$ and $t_{90} = \ln 10/k$, which supports the selection of a minimum HRT [3] (Table 14). In operational terms, k enables a rapid assessment of whether a given batch requires a longer HRT or a more cautious OLR ramp-up. A higher ADL more often indicates slower kinetics, reflected in a lower k, than a reduced final methane potential. This distinction has direct implications for batch blending and feeding schedules.

To assign a clear process meaning to the kinetic parameters, they were evaluated against analytically determined silage characteristics. These included carbohydrate and fibre fractions (ADF/ADL), dry matter and mineral content, physicochemical properties (pH and EC), and indicators of nutrient balance and trace element supply (C/N, Ni/Co/Mo/Se). This approach helps identify which feedstock properties primarily determine methane potential (G_{max}/G_∞) and which control the time course of conversion, including start-up delay (λ) and effective conversion rate (R_{max}, k). The most consistent relationships observed across the analysed batches are summarised below:

- Carbohydrate fractions (Tables 6 and 7): Higher residual OM and hemicellulose correspond to a shorter λ, higher R_{max} (Gompertz), and higher k (Cone). Higher cellulose and, in particular, higher ADL are associated with slower late-stage conversion, a lower k, and a flatter second half of the trajectory.
- DM/volatile solids/ash (Table 3): These factors mainly affect the yield on a fresh-matter basis and energy density. Ash dilutes the biodegradable load and is often accompanied by a lower k, whereas a higher organic fraction supports higher G_{max} and G_∞. Differences on a fresh-matter basis therefore reflect both kinetics (k) and DM and the OM/DM share, which should be considered in logistics and dosing.
- pH/EC (Table 2): After dilution, silage pH does not typically limit the process. Higher EC, linked to Na/Cl/S (Table 10), increases λ and reduces k. This effect is mitigated by batch blending and by maintaining alkalinity at 3–5 g $CaCO_3$/L. Elevated EC is not synonymous with toxicity, but it signals the need for controlled feeding, gradual introduction of the highest-EC batches, preferential mixing with lower-EC material, and, where appropriate, rapid verification of the K/Na/Cl ionic profile under operating conditions.
- CP–CL–CF (Table 5): Moderate CL may favour methane content, whereas CF (Weende) is only indicative. Fibre recalcitrance is better captured by ADF/ADL, which is reflected in k and in the late-stage shape of the curve. The results support the view that fibre architecture (ADF/ADL) is a more informative descriptor of kinetics than CF, particularly when BMP/VS remains high despite elevated fibre content.
- C/N and trace elements (Tables 8 and 12): A lower C/N shortens λ but requires control of TAN/FAN. A higher C/N reduces ammonia-related risk and supports conversion

completion. Ni/Co/Mo/Se stabilise methanogenesis and typically support a shorter λ and sustained R_{max}. No clear deficiencies in ultra-trace elements were evident in this dataset. Differences among batches may nonetheless support blending strategies, for example, combining material richer in Ni and Co with batches that have a more favourable fibre structure and higher hemicellulose.

- Biogas quality and conversion extent (Table 10): Methane content and OM/VS conversion provide independent confirmation that batches with higher BMP/VS tend to achieve deeper degradation. A more favourable share of energy-rich fractions, such as lipids, may also increase methane content even when fibre hydrolysis is slower.

From a digester-operation standpoint, the key requirement is to translate model parameters into decisions on batch introduction, OLR ramp-up, blending strategy, and the minimum hydraulic retention time needed to reach conversion completion. Because the Gompertz and Cone (m = 1) models capture different aspects of the BMP curves, their use should reflect the operational objective. The Gompertz model is more informative for start-up control and sensitivity to inhibiting factors, including osmotic pressure. The Cone model supports rapid batch comparison and practical inference on required HRT via k and derived characteristic times. The operational recommendations can therefore be summarised as follows:

- Use the modified Gompertz model when the lag phase is relevant or when the BMP curve is asymmetric, because λ and R_{max} support start-up control and OLR ramp-up decisions.
- Use the first-order Cone model (m = 1) for rapid benchmarking across batches and for HRT planning when the trajectory is close to mono-exponential, because k directly determines t_{50} and t_{90} [3].
- Batches with elevated ADL should be managed with a longer HRT and a more conservative OLR ramp-up, because lignin predominantly slows kinetics rather than reducing the final BMP.
- Batches with elevated EC should be introduced gradually and preferentially blended with lower-EC material, because osmotic stress may extend λ and reduce short-term stability.
- The C/N ratio should be maintained at a level that limits TAN/FAN risk while avoiding nitrogen limitation, because C/N primarily affects process robustness during start-up and load changes.
- Higher residual OM and hemicellulose indicate faster early-stage conversion and higher k or R_{max}; therefore, these batches can support kinetics in blends, but they require controlled feeding to avoid short-term VFA accumulation.

These rules of thumb provide a practical link between the fitted kinetic parameters and day-to-day decisions on batch introduction, blending, OLR ramp-up, and minimum HRT.

The modelling approaches applied here (Gompertz and the first-order Cone model with m = 1) reproduce the BMP test signal for maize silage most faithfully and provide a clear basis for operational decisions on organic loading rate, hydraulic retention time, and feedstock blending. Provided that the curves do not exhibit a pronounced, prolonged induction phase or an ambiguous bimodal rate pattern, expanding the modelling framework does not yield an objective improvement in inference quality and instead increases estimation uncertainty. Within these bounds, the Gompertz plus Cone (m = 1) combination remains the most informative, robust, and practical option for the analysed batches in the context of anaerobic digestion [1,4]. In summary, the kinetics of maize silage anaerobic digestion are governed by the balance between readily fermentable fractions, which drive rapid early production and higher R_{max}, and fibre-hydrolysis resistance, which shapes late-stage tailing and the effective rate constant k; for this reason, parallel use of the Gompertz model to assess start-up behaviour and salinity sensitivity (λ, R_{max}) and the Cone

model (m = 1) for rapid batch benchmarking and HRT selection (G_∞, k, and the derived t_{50} and t_{90}) is recommended (see Table 14), whereas for batches showing a distinct induction phase or a rate change indicative of two-fraction behaviour, it is justified to treat Gompertz as the primary tool or to adopt two-fraction extensions, although in the present dataset the Gompertz plus Cone approach provides the best compromise between interpretability, estimation stability, and operational usefulness.

5. Conclusions

In this study, the methane potential and the kinetic course of methane fermentation of maize silage were assessed using BMP tests, physicochemical characterisation, and kinetic model fitting. The results confirm that both the final BMP and the rate of CH_4 accumulation depend on the interaction between readily fermentable fractions and structural constraints on fibre hydrolysis, which has direct implications for operational strategy in biogas plants. Accordingly, the key conclusions are as follows:

1. The analysed silages showed good, process-relevant variation in methane yields: BMP on a VS basis ranged from approximately 336 to 402 m^3 CH_4/Mg VS, with clear leaders in organic matter quality (E, C, and G).
2. Differences in yields expressed on a fresh-matter basis were largely governed by dry matter (DM) content, supporting reporting results both on an FM basis and after normalisation to DM and VS to distinguish dilution effects from the quality of the biodegradable fraction.
3. Indicators of biogas quality and the extent of organic matter degradation were internally consistent: the CH_4 share in biogas was approximately 52.1–56.8%, and organic matter conversion was approximately 74.6–85.8%, with differences that are relevant for operation.
4. First-order kinetics (Cone, m = 1) indicate a rapid early phase and a moderately long tail towards completion: for samples A–J, k was approximately 0.058–0.069 d^{-1}, giving t_{50} values of about 10–12 days and consistent with the observed timing of half conversion.
5. From a practical perspective, retention windows of 40–50 days allow near-complete realisation of BMP potential, whereas batches with elevated electrical conductivity (EC; e.g., J) should be managed more conservatively through feedstock blending and controlled increases in OLR, even though EC alone does not determine toxicity.

Maize silage performance in anaerobic digestion is therefore best interpreted through the interplay between readily fermentable fractions and fibre recalcitrance, which primarily governs conversion rate rather than ultimate methane potential. The modified Gompertz and first-order Cone models provide a coherent basis for routine batch benchmarking and support operational decisions on loading strategy, retention time, and feedstock blending under variable fibre composition and salinity.

Author Contributions: Conceptualisation, K.P.; formal analysis, K.P., A.A.P. and M.B.P.; resources, K.P., A.A.P. and B.I.; data curation, K.P., M.B.P. and B.I.; writing—original draft, K.P.; writing—review and editing, K.P. and A.A.P.; visualisation, K.P.; supervision, K.P. and M.B.P. All authors have read and agreed to the published version of the manuscript.

Funding: The research was conducted as part of the authors' independent scientific research, in cooperation with the company Biolab—Energy A&P (Poznań, Poland).

Data Availability Statement: The data presented in this study are available from the corresponding author upon reasonable request and subject to confidentiality restrictions. Raw data are not publicly available.

Conflicts of Interest: The authors declare no conflicts of interest.

References

1. Sarode, S.D.; Kumar, D.; Mathias, D.; McNeill, D.; Kaparaju, P. Anaerobic Digestion of Spoiled Maize, Lucerne and Barley Silage Mixture with and without Cow Manure: Methane Yields and Kinetic Studies. *Energies* **2023**, *16*, 6179. [CrossRef]
2. Economou, E.A.; Dimitropoulou, G.; Prokopidou, N.; Dalla, I.; Sfetsas, T. Anaerobic Digestion Remediation in Three Full-Scale Biogas Plants through Supplement Additions. *Methane* **2023**, *2*, 265–278. [CrossRef]
3. Li, P.; Li, W.; Sun, M.; Xu, X.; Zhang, B.; Sun, Y. Evaluation of Biochemical Methane Potential and Kinetics on the Anaerobic Digestion of Vegetable Crop Residues. *Energies* **2019**, *12*, 26. [CrossRef]
4. Wu, G.; Chang, H.; Du, B. Kinetic Modelling of Typical Biological Reactions During Anaerobic Digestion. In *Anaerobic Digestion: Fundamentals, Modelling, and Applications*; Wu, G., Ed.; Green Energy and Technology; Springer: Cham, Switzerland, 2024; pp. 203–223. [CrossRef]
5. Shi, X.-S.; Dong, J.-J.; Yu, J.-H.; Yin, H.; Hu, S.-M.; Huang, S.-X.; Yuan, X.-Z. Effect of Hydraulic Retention Time on Anaerobic Digestion of Wheat Straw in the Semicontinuous Continuous Stirred-Tank Reactors. *Biomed. Res. Int.* **2017**, *2017*, 2457805. [CrossRef] [PubMed]
6. Liu, M.; Wei, Y.; Leng, X. Improving Biogas Production Using Additives in Anaerobic Digestion: A Review. *J. Clean. Prod.* **2021**, *297*, 126666. [CrossRef]
7. Pramanik, S.K.; Suja, F.B.; Porhemmat, M.; Pramanik, B.K. Performance and Kinetic Model of a Single-Stage Anaerobic Digestion System Operated at Different Successive Operating Stages for the Treatment of Food Waste. *Processes* **2019**, *7*, 600. [CrossRef]
8. Kupryaniuk, K.; Witaszek, K.; Vaskina, I.; Filipek-Kaźmierczak, S.; Kupryaniuk, J.; Sołowiej, P.; Dach, J. The Effect of Corn Ensiling Methods on Digestibility and Biogas Yield. *Energies* **2025**, *18*, 188. [CrossRef]
9. Gouveia, B.; Duarte, E.; dos Santos, A.; Fernandes, E. Dual-pool, Three-Phase Kinetic Model of Anaerobic Digestion in Batch Mode. *Heliyon* **2022**, *8*, e09194. [CrossRef]
10. Pererva, Y.; Miller, C.D.; Sims, R.C. Existing Empirical Kinetic Models in Biochemical Methane Potential (BMP) Testing, Their Selection and Numerical Solution. *Water* **2020**, *12*, 1831. [CrossRef]
11. Li, L.; Kong, X.; Yang, F.; Li, D.; Yuan, Z.; Sun, Y. Biogas Production Potential and Kinetics of Microwave and Conventional Thermal Pretreatment of Grass. *Appl. Biochem. Biotechnol.* **2012**, *166*, 1183–1191. [CrossRef]
12. Dell'Omo, P.P. Different Susceptibilities of Wheat Straw and Corn Stover to Mechanical Pretreatment for Biomethane Production. *Methane* **2025**, *4*, 5. [CrossRef]
13. *Norm VDI 4630*; Fermentation of Organic Materials Characterization of the Substrate, Sampling, Collection of Material Data, Fermentation Tests. German Engineers Club: Düsseldorf, Germany, 2006.
14. *DIN Guideline 38 414-S8*; Characterisation of the Substrate, Sampling, Collection of Material Data, Fermentation Tests. German Institute for Standardization: Berlin, Germany, 1985.
15. Pilarski, K.; Pilarska, A.A.; Boniecki, P.; Niedbała, G.; Durczak, K.; Witaszek, K.; Mioduszewska, N.; Kowalik, I. The efficiency of industrial and laboratory anaerobic digesters of organic substrates: The use of the Biochemical Methane Potential Correction Coefficient. *Energies* **2020**, *13*, 1280. [CrossRef]
16. *ISO 10523:2008*; Water Quality—Determination of pH. ISO pH. International Organization for Standardization (ISO): Geneva, Switzerland, 2008. Available online: https://www.iso.org/standard/51994.html (accessed on 11 January 2026).
17. *ISO 11465:1993*; Soil Quality—Determination of Dry Matter and Water Content on a Mass Basis—Gravimetric Method. ISO Dry Matter Content. International Organization for Standardization (ISO): Geneva, Switzerland, 1993. Available online: https://www.iso.org/standard/20886.html (accessed on 11 January 2026).
18. *ISO 7888:1985*; Water Quality—Determination of Electrical Conductivity. International Organization for Standardization (ISO): Geneva, Switzerland, 1985. Available online: https://www.iso.org/standard/14838.html (accessed on 11 January 2026).
19. *ISO 5983-2:2009*; Animal Feeding Stuffs—Determination of Nitrogen Content and Calculation of Crude Protein Content—Part 2: Block Digestion and Steam Distillation Method. International Organization for Standardization (ISO): Geneva, Switzerland, 2009. Available online: https://www.iso.org/standard/52199.html (accessed on 11 January 2026).
20. *ISO 6492:1999*; Animal Feeding Stuffs—Determination of Fat Content. International Organization for Standardization (ISO): Geneva, Switzerland, 1999. Available online: https://www.iso.org/standard/12865.html (accessed on 11 January 2026).
21. *ISO 6865:2000*; Animal Feeding Stuffs—Determination of Crude Fibre Content—Method with Intermediate Filtration. Fibre Crude. International Organization for Standardization (ISO): Geneva, Switzerland, 2000. Available online: https://www.iso.org/standard/13377.html (accessed on 11 January 2026).
22. *ISO 16472:2006*; Animal Feeding Stuffs—Determination of Amylase-Treated Neutral Detergent Fibre Content (aNDF). International Organization for Standardization (ISO): Geneva, Switzerland, 2006. Available online: https://www.iso.org/standard/37898.html (accessed on 11 January 2026).

23. *ISO/IEC Guide 98-3:2008*; Uncertainty of Measurement—Part 3: Guide to the Expression of Uncertainty in Measurement (GUM). ISO: Geneva, Switzerland, 2008.
24. Zwietering, M.H.; Jongenburger, I.; Rombouts, F.M. Modeling of the bacterial growth curve. *Appl. Environ. Microbiol.* **1990**, *56*, 1875–1881. [CrossRef] [PubMed]
25. Hassan, A.N.; Nelson, B.K. Invited Review: Anaerobic Fermentation of Dairy Food Wastewater. *J. Dairy Sci.* **2012**, *95*, 6188–6203. [CrossRef]
26. Pezzolla, D.; Di Maria, F.; Zadra, C.; Massaccesi, L.; Sordi, A.; Gigliotti, G. Optimization of Solid-State Anaerobic Digestion through the Percolate Recirculation. *Biomass Bioenergy* **2017**, *96*, 112–118. [CrossRef]
27. Liang, J.; Li, C.; Luo, L.; Li, D.; Yang, J.; Wong, J.W.C. Deciphering impacts of sulfadiazine on anaerobic co-digestion of pig manure and food waste for methane production. *Bioresour. Technol.* **2025**, *432*, 132671. [CrossRef]
28. Pilarska, A.A.; Pilarski, K. Bioenergy Generation from Different Types of Waste by Anaerobic Digestion. *Energies* **2023**, *16*, 6919. [CrossRef]
29. da Silva, L.M.; de Pinho Costa, K.A.; Gonçalves e Silva, J.A.; Costa, J.V.C.P.; Costa, A.C.; da Costa Severiano, E.; Fernandes, P.B.; Oliveira, K.J.; Mendonça, K.T.M.; Rodrigues, G.O. Fermentative profile and nutritive value of maize, legume and mixed silage. *Semin. Cienc. Agrar.* **2023**, *44*, 1909–1926. [CrossRef]
30. Nurk, L.; Graß, R.; Pekrun, C.; Wachendorf, M. Methane Yield and Feed Quality Parameters of Mixed Silages from Maize (*Zea mays* L.) and Common Bean (*Phaseolus vulgaris* L.). *Bioenerg. Res.* **2017**, *10*, 64–73. [CrossRef]
31. Tangorra, F.; Tugnolo, A.; Schmilovitch, Z.; Calcante, A. On-Site Assessment of Corn Silage Biochemical Methane Potential Using a Cost-Effective NIR Device. *Comput. Electron. Agric.* **2024**, *222*, 109020. [CrossRef]
32. Weide, T.; Duque Baquero, C.; Schomaker, M.; Brügging, E.; Wetter, C. Effects of Enzyme Addition on Biogas and Methane Yields in the Batch Anaerobic Digestion of Agricultural Waste (Silage, Straw, and Animal Manure). *Biomass Bioenerg.* **2020**, *132*, 105442. [CrossRef]
33. Filer, J.; Ding, H.H.; Chang, S. Biochemical Methane Potential (BMP) Assay Method for Anaerobic Digestion Research. *Water* **2019**, *11*, 921. [CrossRef]
34. Pilarska, A.A.; Kulupa, T.; Kubiak, A.; Wolna-Maruwka, A.; Pilarski, K.; Niewiadomska, A. Anaerobic Digestion of Food Waste—A Short Review. *Energies* **2023**, *16*, 5742. [CrossRef]
35. Mirzoyan, N.; Parnes, S.; Singer, A.; Tal, Y.; Sowers, K.; Gross, A. Quality of brackish aquaculture sludge and its suitability for anaerobic digestion and methane production in an upflow anaerobic sludge blanket (UASB) reactor. *Aquaculture* **2008**, *279*, 35–41. [CrossRef]
36. Gavala, H.N.; Yenal, U.; Skiadas, I.V.; Westermann, P.; Ahring, B.K. Mesophilic and Thermophilic Anaerobic Digestion of Primary and Secondary Sludge. Effect of Pretreatment at Elevated Temperature. *Water Res.* **2003**, *37*, 4561–4572. [CrossRef]
37. De Boever, J.L.; Aerts, J.M.; Vanacker, J.M.; De Brabander, D.L. Evaluation of the Nutritive Value of Maize Silages Using a Gas Production Technique. *Anim. Feed Sci. Technol.* **2005**, *123–124*, 255–265. [CrossRef]
38. Cone, J.W.; van Gelder, A.H.; Bachmann, H.; Hindle, V.A. Comparison of Organic Matter Degradation in Several Feedstuffs in the Rumen as Determined with the Nylon Bag and Gas Production Techniques. *Anim. Feed Sci. Technol.* **2002**, *96*, 55–67. [CrossRef]
39. Li, D.; Tang, R.; Yu, L.; Chen, L.; Chen, S.; Xu, S.; Gao, F. Effects of Increasing Organic Loading Rates on Reactor Performance and the Methanogenic Community in a New Pilot Upflow Solid Reactor for Continuously Processing Food Waste. *Renew. Energy* **2020**, *153*, 420–429. [CrossRef]
40. Dasa, K.T.; Westman, S.Y.; Millati, R.; Cahyanto, M.N.; Taherzadeh, M.J.; Niklasson, C. Inhibitory Effect of Long-Chain Fatty Acids on Biogas Production and the Protective Effect of Membrane Bioreactor. *Biomed. Res. Int.* **2016**, *2016*, 7263974. [CrossRef]
41. Michaud, S.; Bernet, N.; Buffière, P.; Delgenès, J.P. Use of the Methane Yield to Indicate the Metabolic Behaviour of Methanogenic Biofilms. *Process Biochem.* **2005**, *40*, 2751–2755. [CrossRef]
42. Jiang, Y.; McAdam, E.; Zhang, Y.; Heaven, S.; Banks, C.; Longhurst, P. Ammonia Inhibition and Toxicity in Anaerobic Digestion: A Critical Review. *J. Water Process Eng.* **2019**, *32*, 100899. [CrossRef]
43. Demichelis, F.; Tommasi, T.; Deorsola, F.A.; Marchisio, D.; Fino, D. Effect of inoculum origin and substrate-inoculum ratio to enhance the anaerobic digestion of organic fraction municipal solid waste (OFMSW). *J. Clean. Prod.* **2022**, *351*, 131539. [CrossRef]
44. Rabii, A.; Aldin, S.; Dahman, Y.; Elbeshbishy, E. A Review on Anaerobic Co-Digestion with a Focus on the Microbial Populations and the Effect of Multi-Stage Digester Configuration. *Energies* **2019**, *12*, 1106. [CrossRef]
45. Kang, X.; Zhang, Y.; Song, B.; Sun, Y.; Li, L.; He, Y.; Kong, X.; Luo, X.; Yuan, Z. The Effect of Mechanical Pretreatment on the Anaerobic Digestion of Hybrid Pennisetum. *Fuel* **2019**, *252*, 469–474. [CrossRef]
46. Gao, Q.; Li, L.; Wang, K.; Zhao, Q. Mass Transfer Enhancement in High-Solids Anaerobic Digestion of Organic Fraction of Municipal Solid Wastes: A Review. *Bioengineering* **2023**, *10*, 1084. [CrossRef]
47. Dandikas, V.; Heuwinkel, H.; Lichti, F.; Drewes, J.E.; Koch, K. Correlation between Biogas Yield and Chemical Composition of Energy Crops. *Bioresour. Technol.* **2014**, *174*, 316–320. [CrossRef]

48. Sayara, T.; Sánchez, A. A Review on Anaerobic Digestion of Lignocellulosic Wastes: Pretreatments and Operational Conditions. *Appl. Sci.* **2019**, *9*, 4655. [CrossRef]
49. Sun, Z.; Liu, Q.; Li, Y.; Mazarji, M.; Feng, L.; Pan, J. Deciphering the Impact of Lignin on Anaerobic Digestion: Focus on Inhibition Mechanisms and Methods for Alleviating Inhibition. *ACS Omega* **2024**, *9*, 44033–44041. [CrossRef]
50. Li, P.; Liu, D.; Pei, Z.; Zhao, L.; Shi, F.; Yao, Z.; Li, W.; Sun, Y.; Wang, S.; Yu, Q.; et al. Evaluation of lignin inhibition in anaerobic digestion from the perspective of reducing the hydrolysis rate of holocellulose. *Bioresour. Technol.* **2021**, *333*, 125204. [CrossRef]
51. Nguyen, V.T.; Beyer, E.; Neumann, J.; Awe, D.; Pfeiffer, W.; Tränckner, J. Anaerobic Treatment of Residuals from Tanks Transporting Food and Fodder. *Environ. Sci. Pollut. Res. Int.* **2019**, *26*, 32698–32707. [CrossRef]
52. Triolo, J.M.; Sommer, S.G.; Møller, H.B.; Weisbjerg, M.R.; Jiang, X.Y. A New Algorithm to Characterize Biodegradability of Biomass during Anaerobic Digestion: Influence of Lignin Concentration on Methane Production Potential. *Bioresour. Technol.* **2011**, *102*, 9395–9402. [CrossRef] [PubMed]
53. Rocamora, I.; Wagland, S.T.; Villa, R.; Simpson, E.W.; Fernández, O.; Bajón-Fernández, Y. Dry anaerobic digestion of organic waste: A review of operational parameters and their impact on process performance. *Bioresour. Technol.* **2020**, *299*, 122681. [CrossRef] [PubMed]
54. González, R.; Peña, D.C.; Gómez, X. Anaerobic Co-Digestion of Wastes: Reviewing Current Status and Approaches for Enhancing Biogas Production. *Appl. Sci.* **2022**, *12*, 8884. [CrossRef]
55. Seid-Mohammadi, A.; Asgari, G.; Shokoohi, R.; Shahbazi, P.; Dargahi, A. Effect of Operation Conditions on Alkalinity Production from Alkaline Substances Used in Anaerobic Wastewater Treatment System. *Desalin. Water Treat.* **2022**, *266*, 62–69. [CrossRef]
56. Yang, H.; Deng, R.; Jin, J.; Wu, Y.; Jiang, X.; Shi, J. Hydrolytic Performances of Different Organic Compounds in Different Lignocellulosic Biomass during Anaerobic Digestion. *Environ. Eng. Res.* **2022**, *27*, 210013. [CrossRef]
57. Arnal-Sierra, R.; Colantoni, S.; Awopone, A.; Boateng, I.; Agyapong, K.; Sarfo, F.K.; Molognoni, D.; Borràs, E. Anaerobic Co-Digestion of Food Waste in Ghana: Biological Methane Potential and Process Stabilisation Challenges in a Rural Setting. *Sustainability* **2025**, *17*, 7590. [CrossRef]
58. Li, W.; Khalid, H.; Zhu, Z.; Zhang, R.; Liu, G.; Chen, C.; Thorin, E. Methane Production through Anaerobic Digestion: Participation and Digestion Characteristics of Cellulose, Hemicellulose and Lignin. *Appl. Energy* **2018**, *226*, 1219–1228. [CrossRef]
59. Lynd, L.R.; Weimer, P.J.; van Zyl, W.H.; Pretorius, I.S. Microbial Cellulose Utilization: Fundamentals and Biotechnology. *Microbiol. Mol. Biol. Rev.* **2002**, *66*, 506–577. [CrossRef]
60. Amin, F.R.; Khalid, H.; Zhang, H.; Rahman, S.U.; Zhang, R.; Liu, G.; Chen, C. Pretreatment Methods of Lignocellulosic Biomass for Anaerobic Digestion. *AMB Express* **2017**, *7*, 72. [CrossRef]
61. Jeihanipour, A.; Niklasson, C.; Taherzadeh, M.J. Enhancement of Solubilization Rate of Cellulose in Anaerobic Digestion and Its Drawbacks. *Process Biochem.* **2011**, *46*, 1509–1514. [CrossRef]
62. Sawatdeenarunat, C.; Surendra, K.C.; Takara, D.; Oechsner, H.; Khanal, S.K. Anaerobic Digestion of Lignocellulosic Biomass: Challenges and Opportunities. *Bioresour. Technol.* **2015**, *178*, 178–186. [CrossRef] [PubMed]
63. Xu, R.; Zhang, K.; Liu, P.; Khan, A.; Xiong, J.; Tian, F.; Li, X. A Critical Review on the Interaction of Substrate Nutrient Balance and Microbial Community Structure and Function in Anaerobic Co-Digestion. *Bioresour. Technol.* **2018**, *247*, 1119–1127. [CrossRef] [PubMed]
64. Mei, W.; Li, L.; Zhao, Q.; Li, X.; Wang, Z.; Gao, Q.; Wei, L.; Wang, K.; Jiang, J. A Critical Review of Effects, Action Mechanisms and Mitigation Strategies of Salinity in Anaerobic Digestion. *Renew. Sustain. Energy Rev.* **2025**, *208*, 115095. [CrossRef]
65. Pabón-Pereira, C.P.; Hamelers, H.V.M.; Matilla, I.; van Lier, J.B. New Insights on the Estimation of the Anaerobic Biodegradability of Plant Material: Identifying Valuable Plants for Sustainable Energy Production. *Processes* **2020**, *8*, 806. [CrossRef]
66. Pilarski, K.; Pilarska, A.A.; Kolasa-Więcek, A.; Suszanowicz, D. An Agricultural Biogas Plant as a Thermodynamic System: A Study of Efficiency in the Transformation from Primary to Secondary Energy. *Energies* **2023**, *16*, 7398. [CrossRef]
67. Salazar-Batres, K.J.; Moreno-Andrade, I. Review of the Effects of Trace Metal Concentrations on the Anaerobic Digestion of Organic Solid Waste. *Bioenerg. Res.* **2025**, *18*, 24. [CrossRef]
68. Li, X.; Huang, J.; Liu, Y.; Huang, T.; Maurer, C.; Kranert, M. Effects of Salt on Anaerobic Digestion of Food Waste with Different Component Characteristics and Fermentation Concentrations. *Energies* **2019**, *12*, 3571. [CrossRef]
69. Zhang, Y.; Jing, J.; Kong, X.; Yuan, J.; Liu, J.; Zhang, C. A Comprehensive Review of the Impact of Trace Elements on Anaerobic Digestion for Organic Solid Wastes. *Proc. Saf. Environ. Prot.* **2024**, *192*, 1172–1189. [CrossRef]
70. Abdelsalam, E.; Samer, M.; Attia, Y.A.; Abdel-Hadi, M.A.; Hassan, H.E.; Badr, Y. Effects of Co and Ni Nanoparticles on Biogas and Methane Production from Anaerobic Digestion of Slurry. *Energy Convers. Manag.* **2017**, *141*, 108–119. [CrossRef]
71. Pobeheim, H.; Munk, B.; Johansson, J.; Guebitz, G.M. Influence of Trace Elements on Methane Formation from a Synthetic Model Substrate for Maize Silage. *Bioresour. Technol.* **2010**, *101*, 836–839. [CrossRef]
72. Wang, Z.; Wang, S.; Zhuang, W.; Liu, J.; Meng, X.; Zhao, X.; Zheng, Z.; Chen, S.; Ying, H.; Cai, Y. Trace Elements' Deficiency in Energy Production through Methanogenesis Process: Focus on the Characteristics of Organic Solid Wastes. *Sci. Total Environ.* **2023**, *878*, 163116. [CrossRef] [PubMed]

73. Erdirencelebi, D.; Kucukhemek, M. Control of Hydrogen Sulphide in Full-Scale Anaerobic Digesters Using Iron (III) Chloride: Performance, Origin and Effects. *Water SA* **2018**, *44*, 176–183. [CrossRef]
74. Pinto-Ibieta, F.; Serrano, A.; Jeison, D.; Borja, R.; Fermoso, F.G. Effect of cobalt supplementation and fractionation on the biological response in the biomethanization of Olive Mill Solid Waste. *Bioresour. Technol.* **2016**, *211*, 58–64. [CrossRef] [PubMed]
75. Romio, C.; Kofoed, M.V.W.; Møller, H.B. Exploring Increased Hydraulic Retention Time as a Cost-Efficient Way of Valorizing Residual Biogas Potential. *Bioresour. Technol.* **2023**, *387*, 129646. [CrossRef]
76. Wang, Y.; Chen, Y.; Xie, H.; Cao, W.; Chen, R.; Kong, Z.; Zhang, Y. Insight into the Effects and Mechanism of Cellulose and Hemicellulose on Anaerobic Digestion in a CSTR-AnMBR System during Swine Wastewater Treatment. *Sci. Total Environ.* **2023**, *869*, 161776. [CrossRef]
77. Zhang, N.; Wu, C.; Zhang, J.; Han, S.; Peng, Y.; Song, X. Impacts of Lipids on the Performance of Anaerobic Membrane Bioreactors for Food Wastewater Treatment. *J. Membr. Sci.* **2023**, *666*, 121104. [CrossRef]
78. Ferdeș, M.; Paraschiv, G.; Ionescu, M.; Dincă, M.N.; Moiceanu, G.; Zăbavă, B.Ș. Anaerobic Co-Digestion: A Way to Potentiate the Synergistic Effect of Multiple Substrates and Microbial Diversity. *Energies* **2023**, *16*, 2116. [CrossRef]
79. Wu, H.-M.; Li, X.; Chen, J.-N.; Yan, Y.-J.; Kobayashi, T.; Hu, Y.; Zhang, X. Food Waste Anaerobic Digestion Under High Organic Loading Rate: Inhibiting Factors, Mechanisms, and Mitigation Strategies. *Processes* **2025**, *13*, 2090. [CrossRef]
80. Qian, C.; He, S.; Li, X.; Wu, S.; Wang, D.; Yang, C. Effects of Salinity on Anaerobic Digestion: Performance, Microbial Physiology, and Community Dynamics. *Bioresour. Technol.* **2025**, *431*, 132619. [CrossRef]
81. Massaccesi, L.; Sordi, A.; Micale, C.; Cucina, M.; Zadra, C.; Di Maria, F.; Gigliotti, G. Chemical Characterisation of Percolate and Digestate during the Hybrid Solid Anaerobic Digestion Batch Process. *Process Biochem.* **2013**, *48*, 1361–1367. [CrossRef]
82. Zhang, H.; An, D.; Cao, Y.; Tian, Y.; He, J. Modeling the Methane Production Kinetics of Anaerobic Co-Digestion of Agricultural Wastes Using Sigmoidal Functions. *Energies* **2021**, *14*, 258. [CrossRef]
83. Oslaj, M.; Mursec, B.; Vindis, P. Biogas Production from Maize Hybrids. *Biomass Bioenergy* **2010**, *34*, 1538–1545. [CrossRef]
84. Mohammadianroshanfekr, M.; Pazoki, M.; Pejman, M.B.; Ghasemzadeh, R.; Pazoki, A. Kinetic Modeling and Optimization of Biogas Production from Food Waste and Cow Manure Co-Digestion. *Results Eng.* **2024**, *24*, 103477. [CrossRef]
85. Steiniger, B.; Hupfauf, S.; Insam, H.; Schaum, C. Exploring Anaerobic Digestion from Mesophilic to Thermophilic Temperatures—Operational and Microbial Aspects. *Fermentation* **2023**, *9*, 798. [CrossRef]
86. Lower, L.; Qiu, Y.; Sartor, R.C.; Sagues, W.J.; Cheng, J.J. Kinetic Modeling of Thermophilic Anaerobic Digestion of Lemnaceae for Biogas Production. *Bioenerg. Res.* **2025**, *18*, 23. [CrossRef]
87. Almomani, F.; Bhosale, R.R. Enhancing the Production of Biogas through Anaerobic Co-Digestion of Agricultural Waste and Chemical Pre-Treatments. *Chemosphere* **2020**, *255*, 126805. [CrossRef]